EUROPEAN ORGANIZATION FOR NUCLEAR RESEARCH

HR/ml CERN/PS/84-10 (AA)

STUDIES OF A PLASMA LENS WITH PSEUDO-SPARK GEOMETRY FOR APPLICATION IN HIGH ENERGY PARTICLE ACCELERATORS

J. Christiansen*, K. Frank*, H. Riege**, R. Seeböck***

*) Phys. Inst. Univ. Erlangen-Nürnberg

**) CERN, Geneva

***) Siemens AG, ZFE, Erlangen

Paper presented at the Tagung der Deutschen Physikalischen Gesellschaft,
Kiel, 20-23 March, 1984

Geneva, Switzerland
28 May 1984

Abstract

Linear "wire"-lenses are ideal collecting devices for high energy particles emerging from a target. Optimum yields are expected, if the current carrying medium is a plasma column in z-pinch configuration. A pulse generator featuring 20 kJ, 12 kV and up to 200 kA has been set up to study the influence of gas-type, gas pressure and preionisation on breakdown delay, jitter and pinch dynamics by current, voltage, field and streak camera measurements. Electrodes with pseudo-spark geometry are used to reduce internal resistance and electrode destruction and to stabilize the pinch. The test results lead to a design of a prototype lens for the CERN antiproton source.

1. Introduction

The present daily antiproton collection and accumulation rate for $\bar{p}$-physics at the SPS-collider and at LEAR will be increased by at least a factor of 10. A larger production cone of antiprotons (transversal acceptance = 200 mm mrad and $\Delta p/p = 0.06$) has to be transferred to the future ACOL-ring. Hence a much stronger "wire" lens is needed for $\bar{p}$-collection instead of the actually used magnetic horn. A wire lens is essentially a cylindrical conductor passed by a high current of uniform density in axial direction. The resulting linear B_θ- field leads to simultaneous focalization in both transversal planes. Such a lens is also foreseen for focusing the protons coming from the PS to the $\bar{p}$-production target (Fig. 1).
Two ways of realizing linear lenses are now pursued at CERN:

a) The conductor consists of a solid or liquid lithium rod (lithium lens).

b) The current carrying medium is a low pressure plasma column (plasma lens).

Although Li is the least absorbing solid material the $\bar{p}$-losses in a 10cm long lithium cylinder already exceed 10%. The non-absorbing plasma lens can be made longer and, while achieving the same focusing effect, can be run at a lower current. A 10cm long lithium lens pulsed with 1 MA peak current can therefore be replaced by a plasma lens of equal diameter and 30 cm length pulsed with only 350 kA current amplitude.
In a low pressure plasma lens the $\bar{p}$ absorption can, except from end cap losses, be neglected. The current densities in the electrodes and return conductors are relatively small and mechanical and magnetic forces on the quartztube and the electrodes are not important. The current penetration time in a plasma can be controlled. The current pulse needs to flow for a few microseconds only. The stored energy in the capacitor bank can be fully used, provided the plasma lens layout is chosen such,that the maximum discharge current coincides with the required operating current for $\bar{p}$ collection. The main problem of the plasma lens is the energy dissipation inside the plasma vessel leading to electrode damage by evaporation and sputtering and to a deterioration of the insulator surface by radiation (IR to soft X-ray) and deposition of evaporated metal.
For both types of lenses the life-time limitations have to be overcome by the proper choice of materials, configuration and cooling devices. The plasma lens design requires in addition the knowledge of the pinch dynamics and of its control. Contrary to the lithium lens instabilities like turbulences, "kink" and "sausage" instabilities, may lead to irreproducible focusing results and have to be avoided. The work described in this report is mainly concerned with the basic problems of energy dissipation in the plasma lens and with the dynamics and stability of the pinching process. From experimental results obtained with a preliminary prototype lens and test generator we established scaling laws necessary to design a plasma lens taylored to a specific application.

The life-testing of a plasma lens under real operating conditions and the measurement of magnetic field distribution inside the quartz tube will be the aim of the next development stage, which has started now and will be described elsewhere.

Two cases of applications of plasma lenses in high energy physics are known from Berkeley[1] and Brookhaven[2]. Whereas the Berkeley focussing device was rather modest with respect to the power involved, the performance of the BNL plasma lens, realized in 1965, came rather near to what will be required for ACOL. The BNL lens was successfully working for 24 hours beam time in the AGS and produced a net gain in neutrino events.

2. The prototype plasma lens

2.1 Configuration of the plasma lens

It is our aim to develop a system in which the azimuthal B_θ- field of a current carrying self-pinching plasma column serves for high energy particle focussing. Fig. 2 shows the principal scheme of such a z-pinch device. Under the influence of the magnetic self-field the plasma shell will be symmetrically compressed towards the axis of the quartz cylinder and extends longitudinally between the hollow anode and cathode electrodes. We call such a geometry pseudo-spark structure[3]. Though the typical effects of the pseudo-spark are only observed during the initial break-down phase, we believe that such a structure has also some advantages for later discharge phases. Longitudinal plasma shockwaves can easily expand into the hollow electrode spaces. The energetic electron beam through the anode can be deviated electrostatically by the insertion of an insulating end-cap facing the anode hole. This has the further advantage of decreasing even more the absorption of antiprotons The electrode center hole diameter is determined by the maximum angle of the p-cone to be captured. It should correspond to the pinch diameter at $\bar{p}$ production time. The current has to enter and leave the plasma column through symmetrically arranged return conductors and stripline connections.

Table 1 shows the main features of the first prototype and the possible data of a later real plasma lens. The linearity of current density with radius should be better than 10% and stability of the discharge is required during the 450 ns of $\bar{p}$ production time. A photo of the first plasma lens prototype is shown in Fig. 3.

TABLE 1

	First prototype	Real plasma lens
Length of quartz cylinder	200 mm	270 mm
Inner diameter of quartz cylinder	40 mm	190 mm
Electrode hole diameter	20-25 mm	20-40 mm
Pinch diameter	3-10 mm	20-40 mm
B - field (max)	3 T	5-8 T
B - gradient (max)	600 T/m	100-400 T/m
Current (max)	190 kA	350-450 kA
Time to first pinch phase	2-15 μs	5-7 μs

2.2 Pinch dynamics

Pinching is confinement of a plasma or a conducting liquid by magnetic self-fields. This effect is observed when the magnetic field pressure exceeds the pressure of the conducting medium:

$$\frac{\mu_0 I^2}{8\pi} > n k T \qquad [1] \qquad \text{(Bennett-relation}^5\text{)}.$$

where I is the current, n the number density, and T the medium temperature.

Several models have been developed which approximately describe the pinching process occuring in a typical capacitor discharge circuit (Fig. 4). The sudden compression of a weakly preionized low density plasma by means of a large current lasting for some microseconds has been described by Rosenbluth et al [7]. Assuming a large initial conductivity the skin depth is much smaller than the radius of the plasma column and the current starts to flow in a thin shell on the column surface. The fast rising magnetic pressure drives the shell inward which sweeps up all particles encountered during the movement towards the axis ("snow-plow" model).

When radiation losses, ohmic heating, gas ionization processes and shock waves are neglected we obtain, with the approximation of the one-fluid MHD-momentum equation for infinite plasma conductivity,

$$\partial/\partial t(\rho \vec{v}) + \vec{v}\ \text{grad}\ \rho \vec{v} + \rho \vec{v}\ \ \text{grad}\ \vec{v} = \vec{j} \times \vec{B} - \text{grad}\ p \qquad [2]$$

where: ρ = mass density,
$\vec{v}$ = center of mass velocity,
$\vec{j}$ = current density vector
and $\vec{B}$ = magnetic field vector,

and with Maxwell's equation $\text{curl}\ \vec{B} = \mu_0 \vec{j}$,

the differential equation $$\frac{d}{d\tau}\left[(1 - x^2)\frac{dx}{d\tau}\right] = -\frac{\tau^2}{x} + \alpha x^{-\kappa - 2/3} \qquad [3],$$

where $$x = \frac{\text{radius } r}{\text{quartz tube inner radius } r_0},$$

$$\tau = \frac{\text{time } t}{\text{scaling time for contraction } t_1},$$

$$t_1 = \left[\frac{2\pi}{\mu_0} M_0\right]^{1/4} \left[\frac{r_0}{(dI/dt)_0}\right]^{1/2} \quad \text{(constant current rise)}$$

$$M_0 = \pi r_0^2 \rho_0 \quad \text{(total mass per unit length)}$$

$$\alpha = \frac{2 p_0 \tau^2_{pinch}}{r_0^2 \rho_0}, \quad \text{with } \tau_{pinch} = 1.5\ t_1 = \text{collapse time}$$

and κ = specific heat ratio ($\kappa = 5/3$ for a mono-atomic gas). ρ_0 and p_0 are the initial density and pressure values and the model assumes adiabatic behaviour, pV^{κ}=constant. Fig 5 shows the normalized radius x as a function of normalized time τ for different values of α. From the expression for t_1 we can deduct an approximate scaling law for the pinch time, τ_{pinch} (=time from start of discharge up to the first contraction)

$$\tau_{pinch} \approx r_0 \, (p_0 \, A)^{1/4} \quad (dI/dt)_0^{-1/2} \qquad [4],$$

with A = atomic number.

The prediction of the snow-plow model for the minimum contraction radius is $0 < r_{pinch} < 0.1\ r_0$. This deviates from reality, since generally pinch radii larger than $0.1\ r_0$ are observed. Other models, like the "slug" model[8] or the "energy balance" model[9], predict rather large r_{pinch} -values. During the initial pinch phase only and for pressures < 1mb the snow-plow model is an acceptable approximation. For high pressures above a few mb the other models are nearer to reality. The compression of the plasma column represents a sensible change of inductance and resistance in the discharge circuit and should be observed on the plasma lens current waveform as a dip and on the difference voltage waveform as a peak. In case of a mainly inductive plasma lens the peak voltage is $V_p \approx I \, dL_p/dt$ where L_p is the variable plasma lens inductance. V_p is a maximum when the imploding current shell decelerates and is reflected near the lens axis. Several pinch oscillations may be observed under certain conditions, before thermalization and instabilities like turbulences, lead to a diffuse discharge filling the whole quartz tube. A z-pinch is sensible to instabilities of the so-called "sausage" or "kink" type (Fig. 6). Depending on pressure and gas type the discharge can already be disturbed from the beginning by turbulences. For the plasma lens such instabilities have to the avoided and stable conditions at maximum current during a period of at least 450 ns have to be maintained. An axial B_z - field may considerably improve the discharge stability (Fig. 5) and permits to directly control the pinching parameters τ_{pinch} and r_{pinch}. However, it is desirable to work without B_z, since a second pulse generator would be needed.

2.3 The test pulse generator

Though the performance of the test generator (Fig. 7) used for the first prototype lens investigations was inferior to what will be required for a real plasma lens in future, especially due to its high total inductance and too low peak current, we could study a number of important basic problems and we were able to determine the layout of the next prototype lens. The electrical scheme of the discharge circuit is given in Fig. 8 and its parameters in Table 2.

TABLE 2

Charging voltage	U_0	12 kV
Total storage capacitance	C	281 µF
Total circuit inductance	L_{tot}	0.7 µH (mainly in capacitors)
Maximum energy/pulse	E_{max}	20 kJ
Maximum current with first prototype plasma lens	I_{max}	190 kA in helium at 10 mb
Half wave length	$T_{1/2}$	45 µs

As switches for the lens and the crowbar branch we used either ignitions or pseudo-spark switches. The latter type of switch is more precise (jitter < 20 ns) and can be conveniently incorporated into flat and coaxial strip lines. The plasma lens has to be preionized prior to the main discharge in order to reduce break-down delay and jitter and also initial energy losses due to high internal resistance. Preionization was applied in form of a weak (1mA) dc current and by using the strong leakage current through a saturable inductor incorporated into the main stripline of the circuit. The currents in the circuit were measured with three air-slit transformer coils and the differential voltage accross the plasma lens with two carefully screened high voltage probes.

3. Measurements

As mentionned above we established the priority list of plasma lens problems as follows.

- energy dissipation in the lens
- pinch dynamics
- stability of discharge
- longterm behavior
- B_θ-field measurements

} (not treated in this report)

3.1 Global discharge parameters and waveforms

Though we know that the internal resistance R_i and the inductance L_p of the plasma lens vary during the discharge process we may deduce mean values from the amplitudes, damping factors and phase shifts of the current and differential voltage waveforms. Neglecting the crow-bar (Fig. 8) we have to deal with an R-L-C circuit in the first approximation. Typical average internal resistance values of 10 to 15 mΩ have been measured with the 40 x 200mm prototype lens. Figs. 9 a-f show typical current and differential voltage signals. The effect of pressure and electrode shape on discharge behaviour was studied with helium, argon, nitrogen and xenon as filling gases. In Figs. 10 a and b the results are given for He and Ar. The effect of electrode shape (flat, hollow or multihole) on current amplitude was less than 5%, contrary to what we expected. The reduction of breakdown delay and jitter in the plasma lens under the influence of a weak preionization of 1 mA is shown in Fig. 11. In Ar and He such a weak preionization shortens the breakdown delay in average by a factor of 5.

In order to reduce the initial energy dissipation in the lens a "strong" preionisation was applied by the leakage current (10 to 100A during 1μs) through a series saturable Metglass inductor which was incorporated into the stripline and which saturated after 1μs. The saturable inductor also enables a more efficient use of the circuit crowbar (see Fig. 12).

3.2 Study of pinch dynamics by streak and framing photography

The significance of the dips observed in the current waveforms and the peaks in the voltage waveforms is fully confirmed by optical measurements with a streak camera. This camera allows to take either framing pictures (typically 5 snapshots every 12.5 ns) or streak photographs with streak speeds from ps/cm to ms/cm. Both modes were used. The streak mode is well suited to quantitatively measure the temporal evolution of the pinch, whereas framing photography may reveal spatial and temporal instabilities of the plasma column.

The streak camera measurements were performed with helium, argon, xenon and nitrogen as filling gases in the plasma lens. With argon, xenon and Ar/He, Xe-He mixtures the discharge appeared to be very stable up to and even beyond the first plasma column contraction phase. Nitrogen discharges proved to be less stable especially at pressures below 1 mbar. With helium stability and reproducibility could not be obtained over the whole pressure range from 0.1 to 20 mbar. Here turbulences start to form right from the beginning and persist during the whole discharge cycle (Fig. 13). The excellent spatial and temporal discharge stability in argon is shown by the streak photo of Fig. 14. The spatial stability of the plasma column is also visible in the framing photographs (Fig. 15). In Figs. 16 and 17 the congruence between current and voltage signals and the streak photos of the contracting plasma column is demonstrated with argon and xenon. With increasing pressure minimum pinch radius r_{pinch} and pinch time τ_{pinch} increase as shown in Figs. 18, 19, 20 for argon, xenon and nitrogen. The opposite is true for increasing capacitor charging voltage U_0. In Fig. 21 this effect is given for a 50/50-He/Xe mixture.

4. Discussion

The streak measurements together with the differential voltage signals measured across the plasma lens enable systematic comparisons of the measured pinch times and radii with the behavior predicted from the simple snow-plow model (chap.2.2). The absolute values of r_{pinch} and τ_{pinch} are not reproduced but the scaling according to equ. [4] seems to be valid over a limited parameter range. In Fig. 22 the pinch time is plotted against $p^{1/4}$ and $p_0^{1/2}$. At higher pressures and lower voltages $f(p^{1/2})$ seems to be a better approximation. The same is valid for the pinch radius (Fig. 23). Fig. 24 shows plots of pinch time and pinch radius as function of $U_0^{-1/2}$. Similar results are obtained with xenon as seen in Figs. 25, 26 and 27. The linear dependence of pinch time on the inverse fourth power of atomic number is demonstrated by Fig 28. In all the measurements described above the reproducibility of consecutive discharges is very important. Fig. 29 shows that after opening

the plasma lens at atmospheric pressure several shots are needed to arrive at a reproducible situation. In the results measured on the first prototype lens extrapolations to different discharge conditions (cycling frequency, charging voltage, total circuit inductance, etc) and plasma lens configurations (length, radius) are possible. For a real plasma lens a defined pinch radius
must be obtained at the time of $\bar{p}$ - collection. It is also desirable to get coincidence of pinch time and time to peak current. Free parameters for achieving these requirements are charging voltage, inner plasma lens quartz tube radius, gas pressure and type of gas. The validity of extrapolation was checked with a second prototype lens (Fig. 30) designed for use in the same old pulse generator. The inner diameter of this 250 mm long lens was 236 mm. As shown in Fig. 31 coincidence of the first contraction phase and the maximum current can be easily obtained with this prototype.Internal resistance and plasma temperature of the larger prototype are lower than in the first model. Current densities of typically 50 to 200 kA/cm^2 and internal resistance values of 10 to 15 mΩ are observed in the small prototype, whereas the internal resistance of second prototype is below 10 mΩ and the current density does not exceed 50 kA/cm^2. Details of the measurements the with the second prototype, especially results of magnetic field distribution measurements, are later reported elsewhere.

5. Future plans

A real plasma lens for $\bar{p}$-collection should approximately have the dimensions and electrical specifications given in Table I. The next step of the development programme is the construction of a new pulse generator for testing a prototype lens which would come near to a final real version. The main aim of this phase is the study and improvement of long term behavior under realistic conditions in the laboratory, that is without proton and antiproton beams. We expect problems with electrode erosion and deposition of metal vapor on the quartz tube of the lens. The new pulse generator will have the following features:

Table 3

Maximum peak current	I_{max}	500 kA
Charging voltage	U_o	20-25 kV
Total storage capacitance	C	100 μF
Total circuit inductance	L_{tot}	0.15-0.18 μH
Max energy/pulse	E_{max}	30 kJ
Half wave length	$T_{1/2}$	10-12 μs

Demonstration of sufficient lifetime remains the main subject of this development phase. Only after its successful completion we will be able to recommend the installation of a real plasma lens in the AA and ACOL target area. The life test will be accompanied by thorough measurements of magnetic field distribution B_θ (r,t), current and number density distribution j (r,t), n (r,t) streak and Schlieren photography, etc.

Construction of the new pulse generator starts in September 1984. Progress will depend on available effort. Fortunately we can count on two very fruitful cooperations with the Physical Institute of the University of Erlangen and with the Electrotechnical Institute of the University of Naples.

Acknowlegements

We are grateful to P. Billault, who, in a very competent manner, designed both plasma lens prototypes. We also thank Mr van Gulik for his great help in preparing, setting up, and running the test-set up. The CERN EF-division has kindly provided us with laboratory space, and we especially thank R. Grüb for his constant help during our presence in his area. We are grateful to R. Billinge, who initiated the research on plasma lenses in the PS-division and also to all members of the AA-group, who supported us, especially B. Autin and E. Jones.

We are very much indebted to H. Bluhm from the Institute of Neutronenphysik and Reaktortechnik, KfK., who lent out the streak camera and introduced us into its use.

References:

1) W.K.H. Panofsky and W.R. Baker, The Rev. of Sci.Instr., Vol 21,5 (1950), p.445
2) E.B.Forsyth, L.M. Lederman, Z. Sunderland, IEEE NS-12, Nr.3 (1965), p.872
3) J. Christiansen and C. Schultheiss, Z.Phys. A 290 (1979), p.35
4) D. Bloess et al., NIM, vol. 205,1,2 (1983), p.173
5) W.E. Bennet, Phys. Rev. 45 (1934), p.890
6) N.A. Krall, Principles of plasma physics, Mc Graw Hill (1973)
7) M. Rosenbluth et al., US AEC Report LA - 1850 (1954)
8) D. Potter, Nucl. Fusion 18 6 (1978), p.813
9) S. Lee, Plasma Physics, Vol 25.Nr 5. (1983), p.571

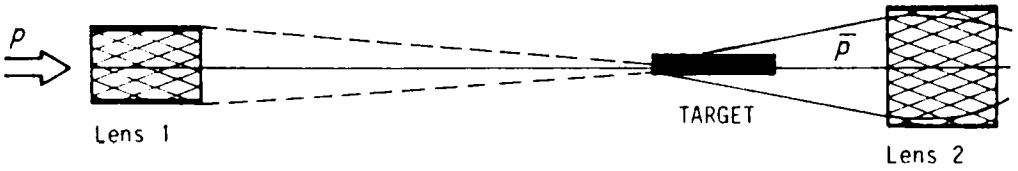

Li:	Plasma:	Li:	Plasma:
375 kA	170 kA	1 MA	370 kA
r = 10 mm	r = 10 mm	r = 20 mm	r = 20 mm
l = 120 mm	l = 270 mm	l = 100 mm	l = 270 mm

Future layout of antiproton collection

Fig. 1

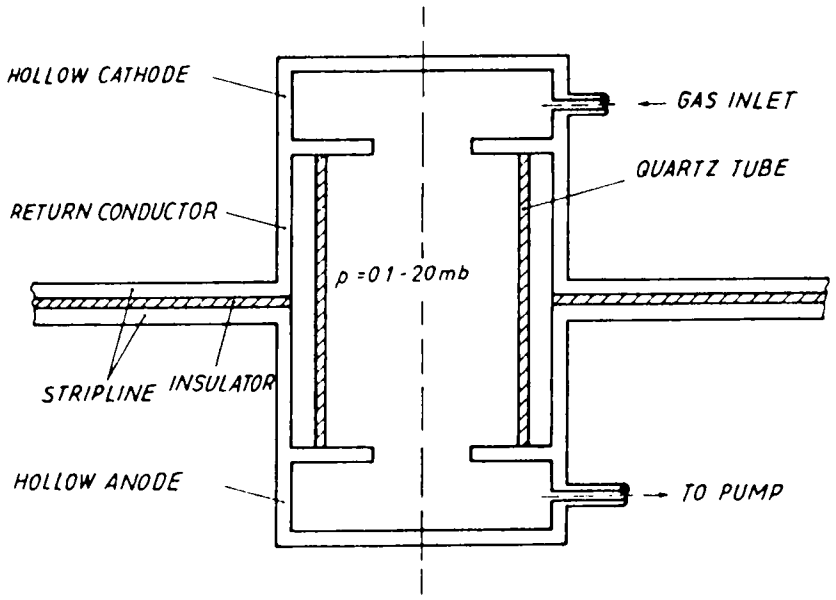

Principle of plasma lens
with pseudo-spark geometry

Fig. 2

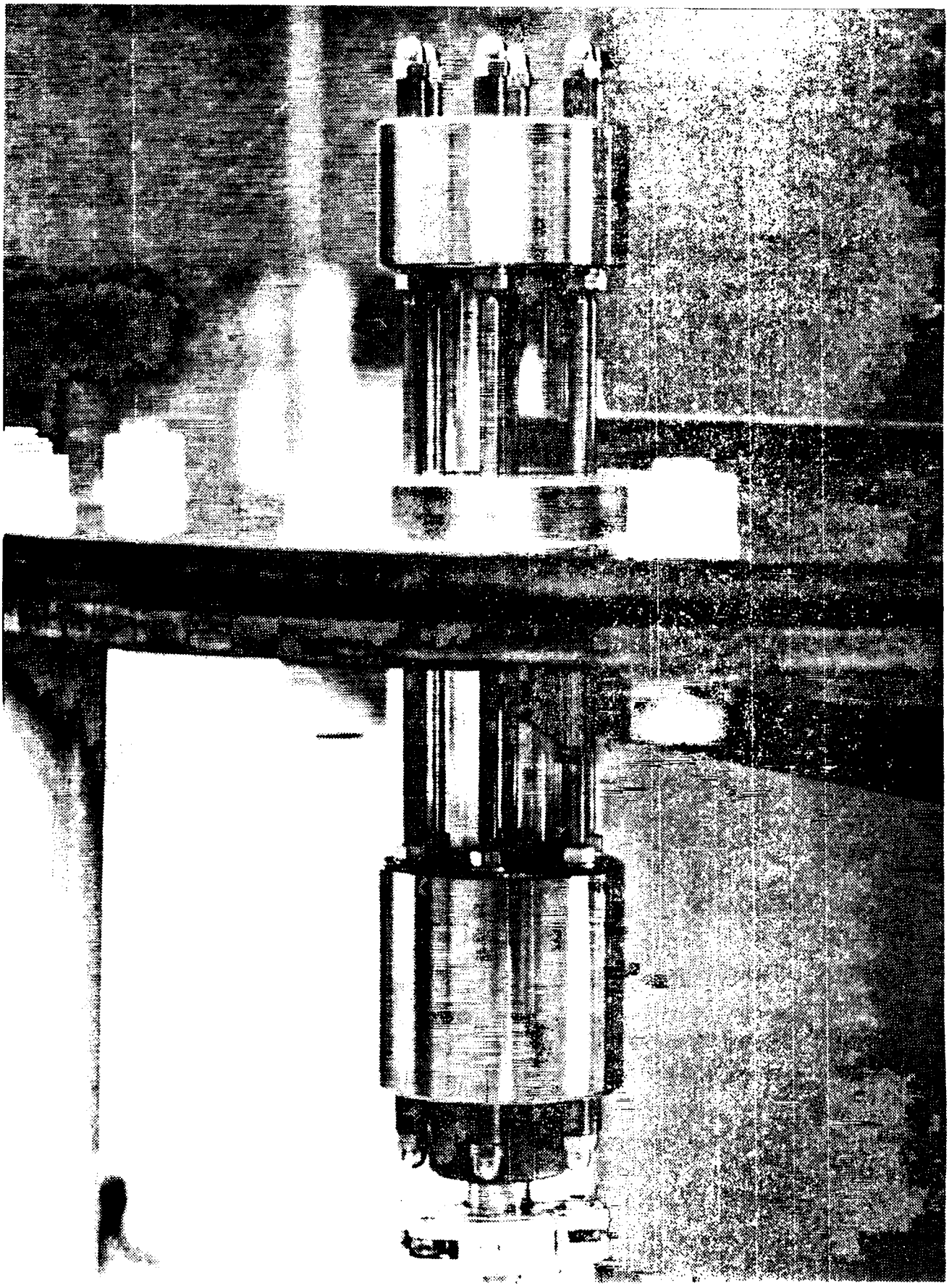

First plasma lens prototype

Fig. 3

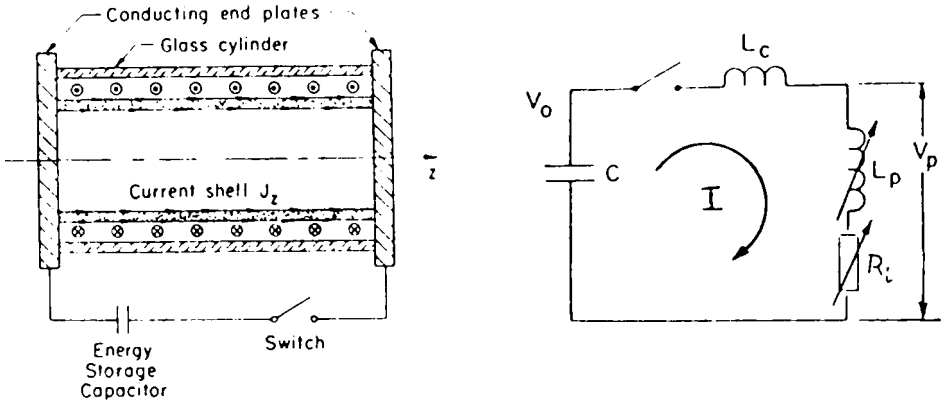

a) b)

a) Schematic of z-pinch (from Ref. 6)

b) Simplified equivalent discharge circuit. The voltage across the plasma lens is $V_p \approx I \left(dL_p/dt + R_i \right)$, where R_i = internal ohmic resistance of the plasma lens.

Fig. 4

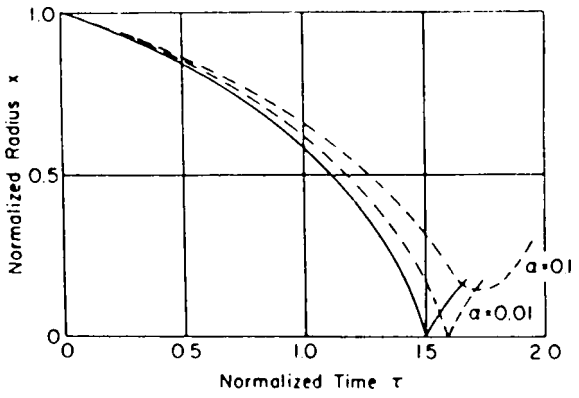

Normalized radius of dynamic-pinch plasma as a function of normalized time showing plasma collapse, or pinch effect (solid curve). Dashed curves show the effect of neutral gas pressure on collapse (from Ref. 6).

Fig. 5

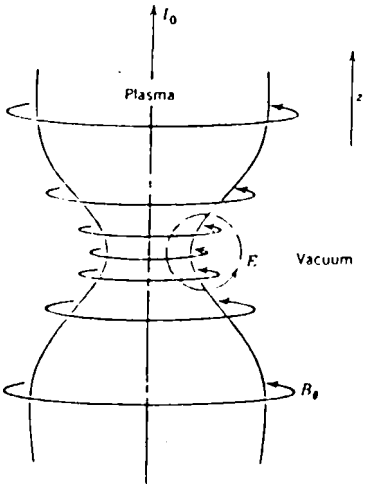

The m = 0 (sausage) instability of the pinch.

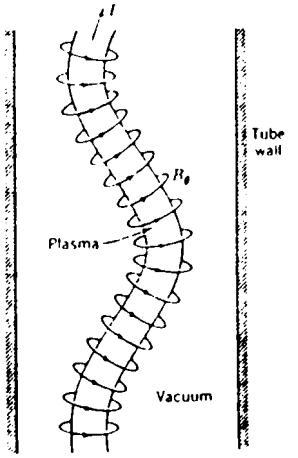

The m = 1 (kink) instability.

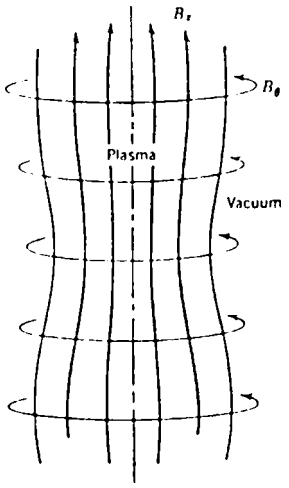

B_z-stabilised pinch

Z-pinch plasma instabilities. Stabilization may be improved by a longitudinal magnetic field B_z, provided that

$$B_\theta/B_z < 2\pi r_p/L$$

Fig. 6

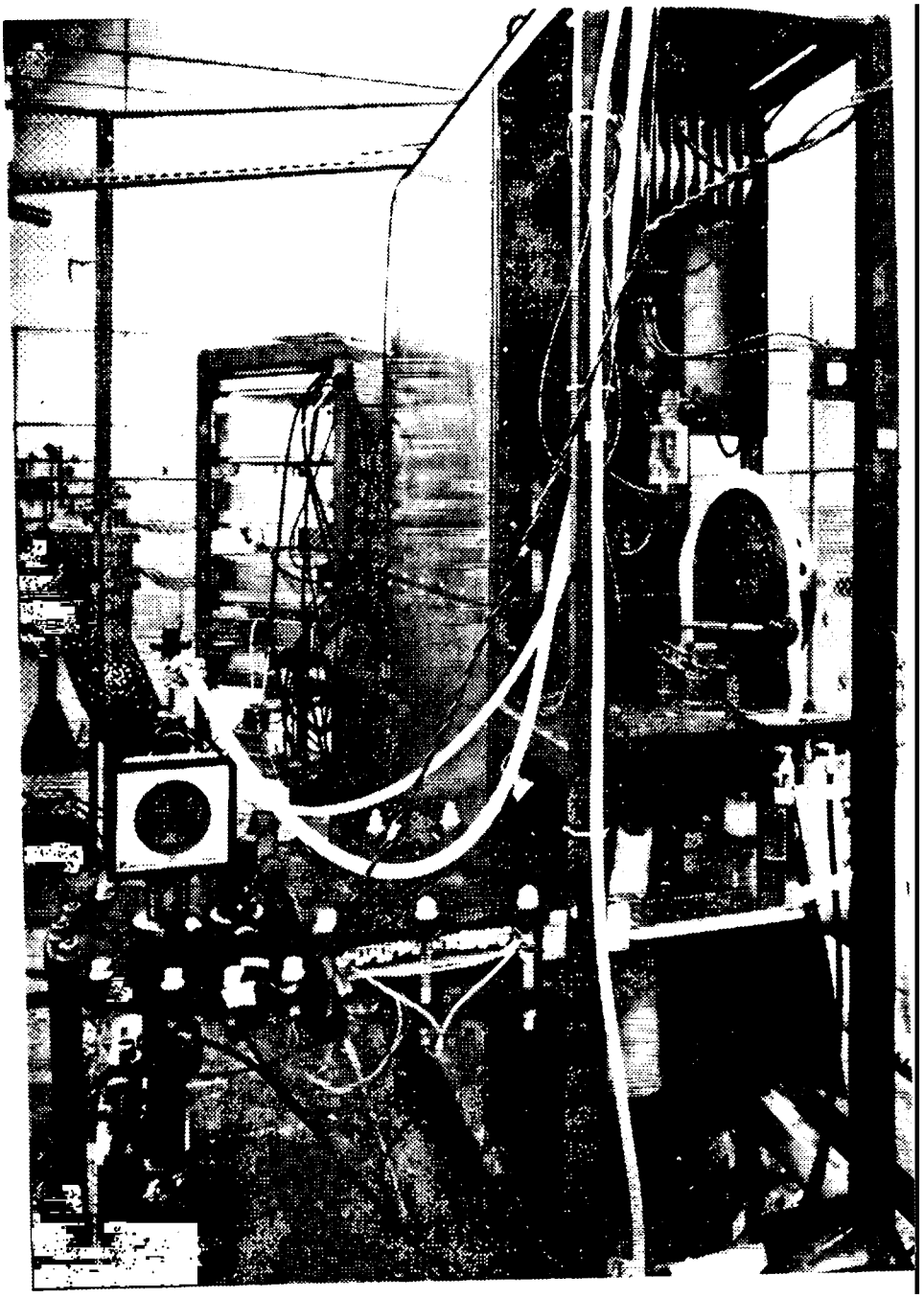

Prototype pulse generator for the first
plasma lens prototype

Fig. 7

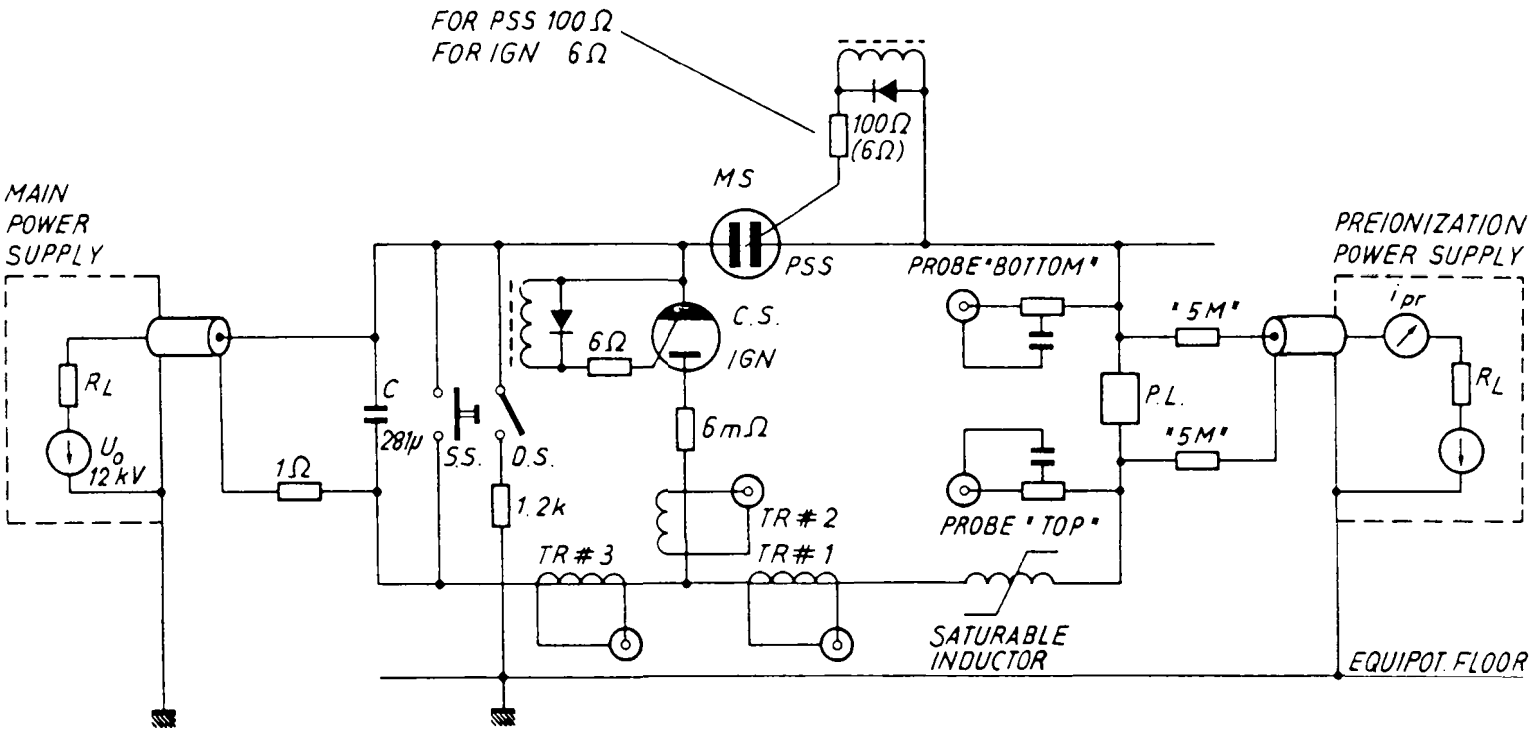

ELECTRICAL SET-UP OF DISCHARGE - CIRCUIT

P.L. = PLASMALENS

C.S. = CROWBAR SWITCH

M.S. = MAIN SWITCH

D.S. = DUMP SWITCH

S.S. = SECURITY SWITCH

R_L = CHARGING RESISTOR

TR # n = MEASURING TRANSISTOR n

IGN = IGNITRON

PSS = PSEUDO-SPARK SWITCH

Fig. 8

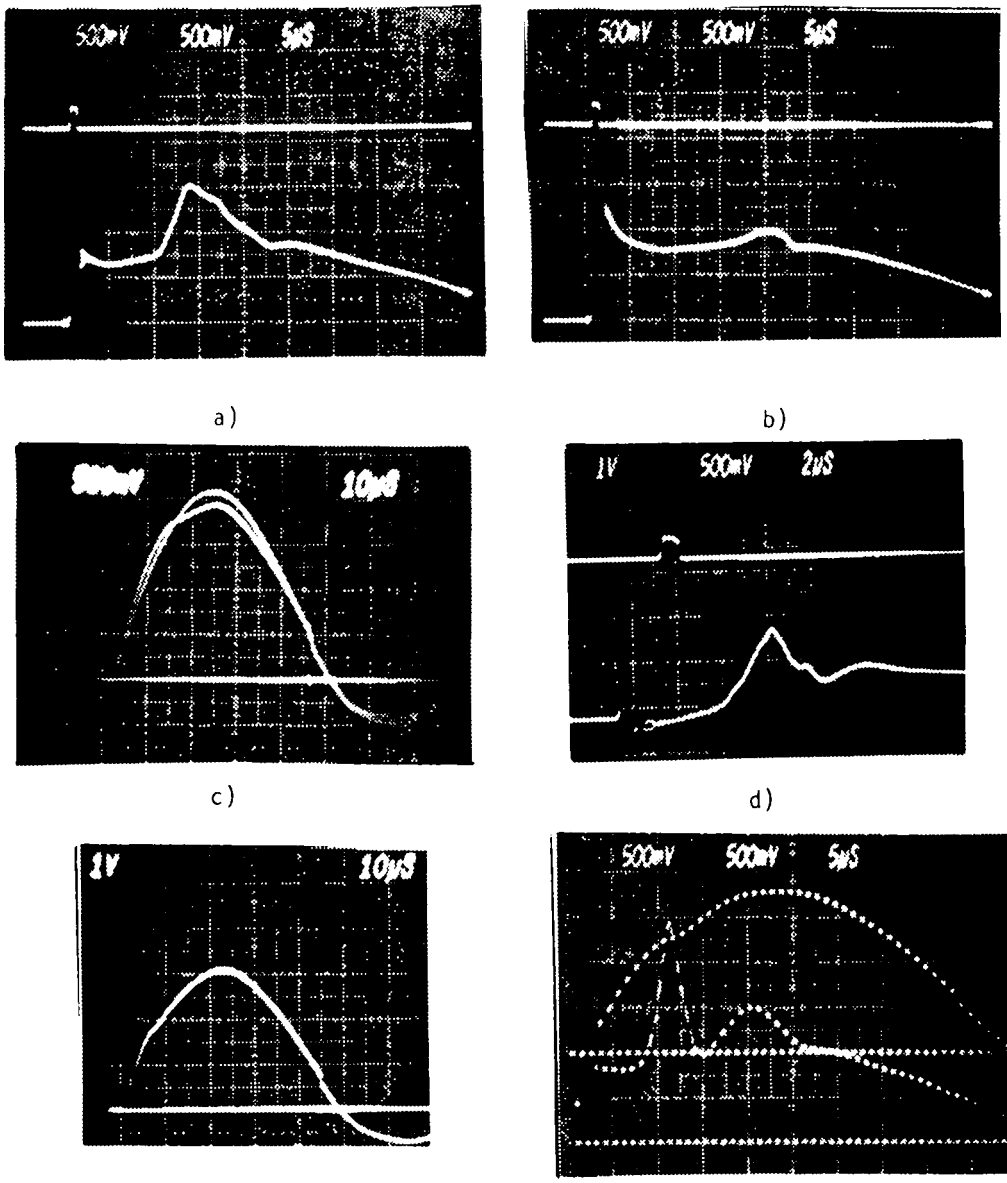

a) b)

c) d)

e) f)

Typical waveforms of current and differential voltage measured with the first plasma lens prototype.

a) Diff. voltage on PL with Xe at 3 mb, U_0 = 4 kV (500 V/div).
b) Diff. voltage on PL with Xe at 10 mb, U_0 = 4 kV (500 V/div).
c) Current through PL with Xe at 3 (below) and 10 (up) mb, U_0 = 4 kV (25kA/Volt).
d) Diff. voltage on PL with Ar at 1.8 mb, U_0 = 6 kV (500 V/div).
e) Current through PL with Ar and 1.8 mb, U_0 = 6 kV (25kA/Volt).
f) Simultaneous diff. voltage and current with Ar at 5mb, U_0 = 5 kV (scaling as above).

Fig. 9

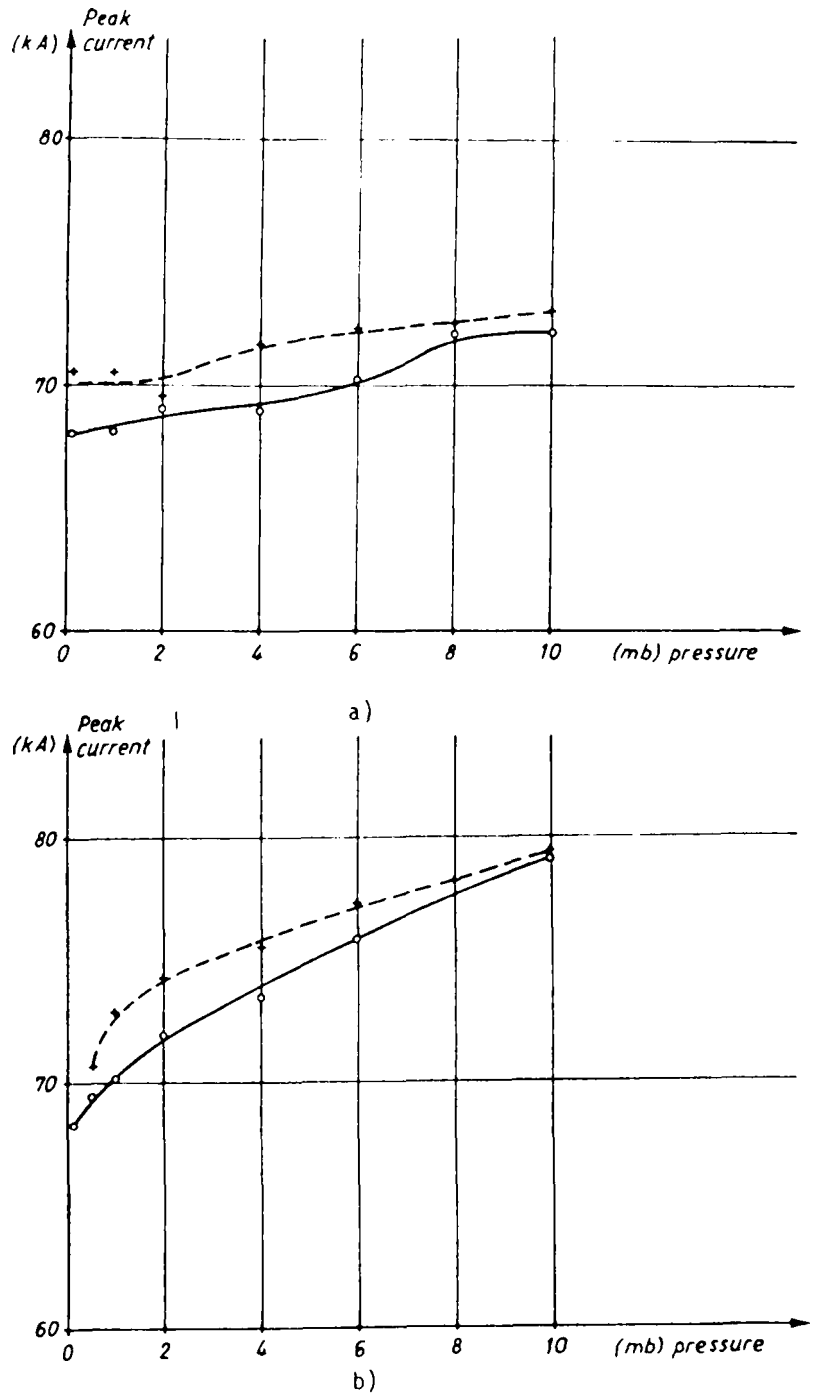

Effect of pressure and electrode shape on peak current.

a) PL filled with Ar, U_o = 5 kV.

b) PL filled with He, U_o = 5 kV.

+ cathode with many small (4 mm diam.) holes.
o cathode with one single centre hole (25 mm diam.).

Fig. 10

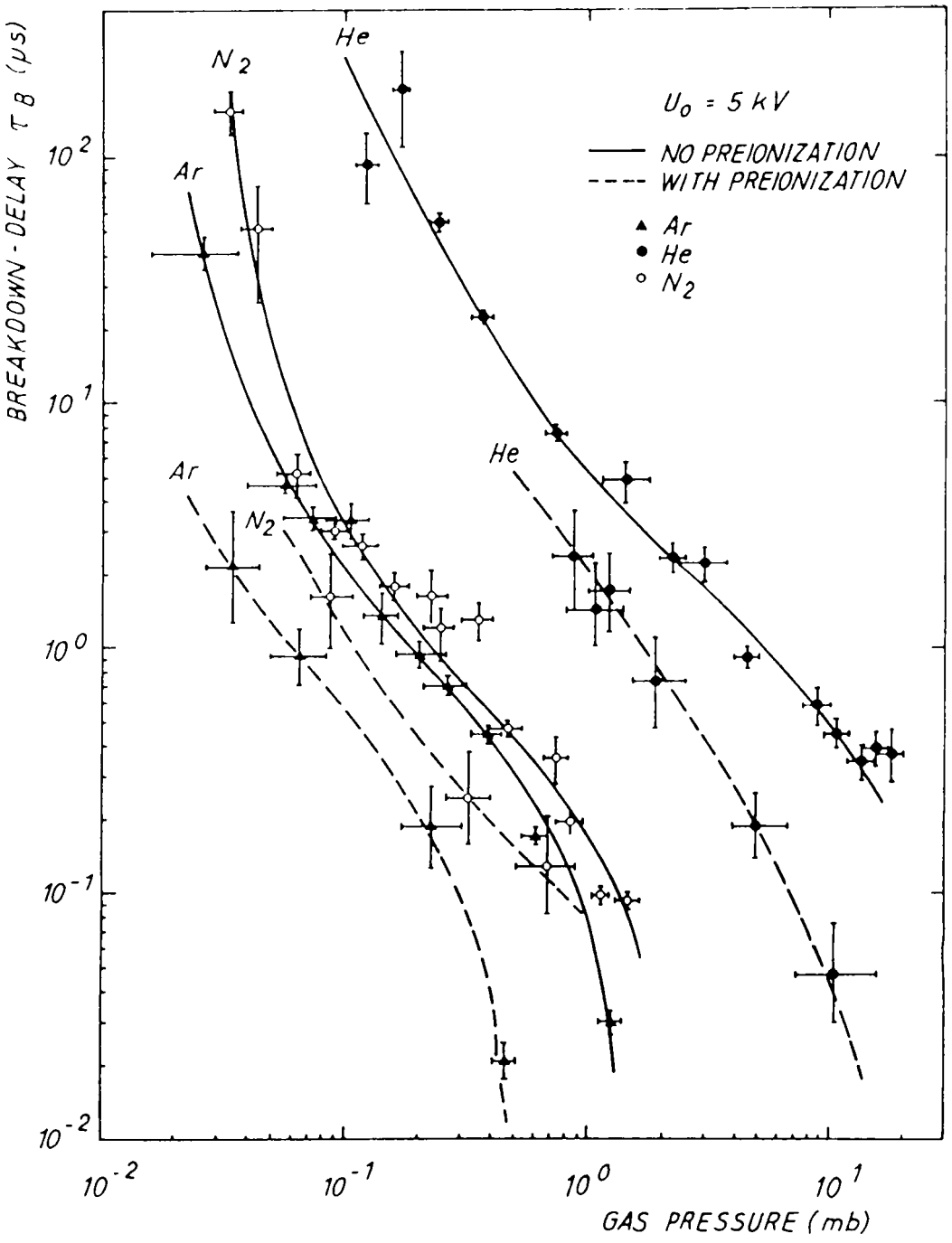

Effect of weak preionization (1mA, 5 kV) on breakdown delay τ_B and jitter of the plasma lens prototype in the Ar and Xe.

Fig. 11

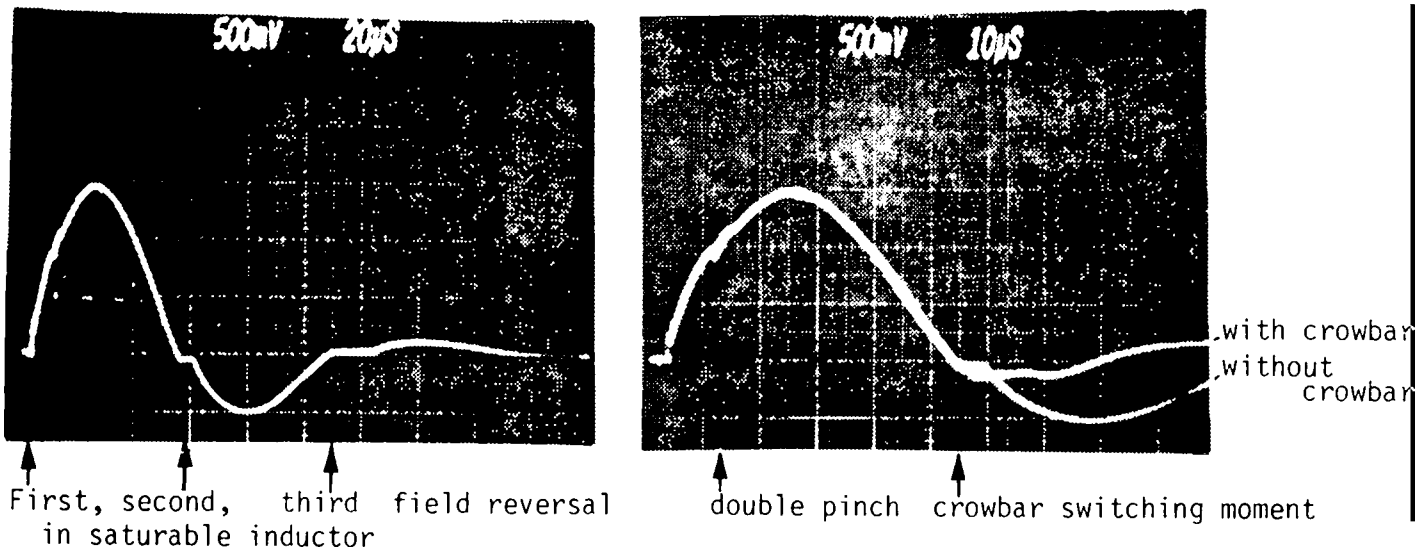

Current waveform of PL with He at 0.8 mb, U_o = 4.5 kV

a) No crowbar switching (37.5 kA/Volt).
b) With crowbar in action and compared with previous case (a).

Fig. 12

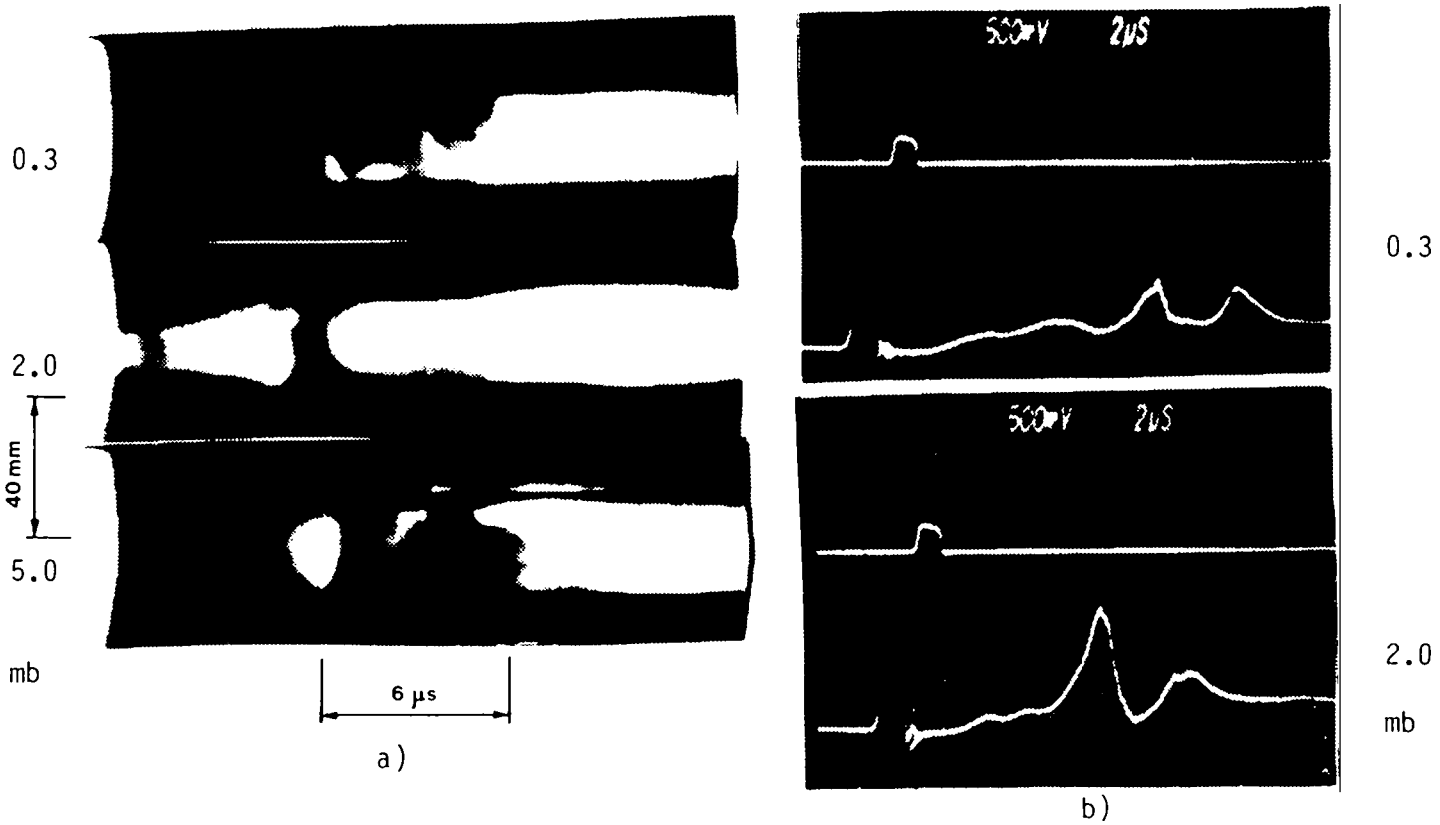

a) Unstable discharge in PL with helium at different pressures photographed with a streak camera (streak speed 3μs/cm U_o = 4 kV)
b) Corresponding differential voltage waveforms

Fig. 13

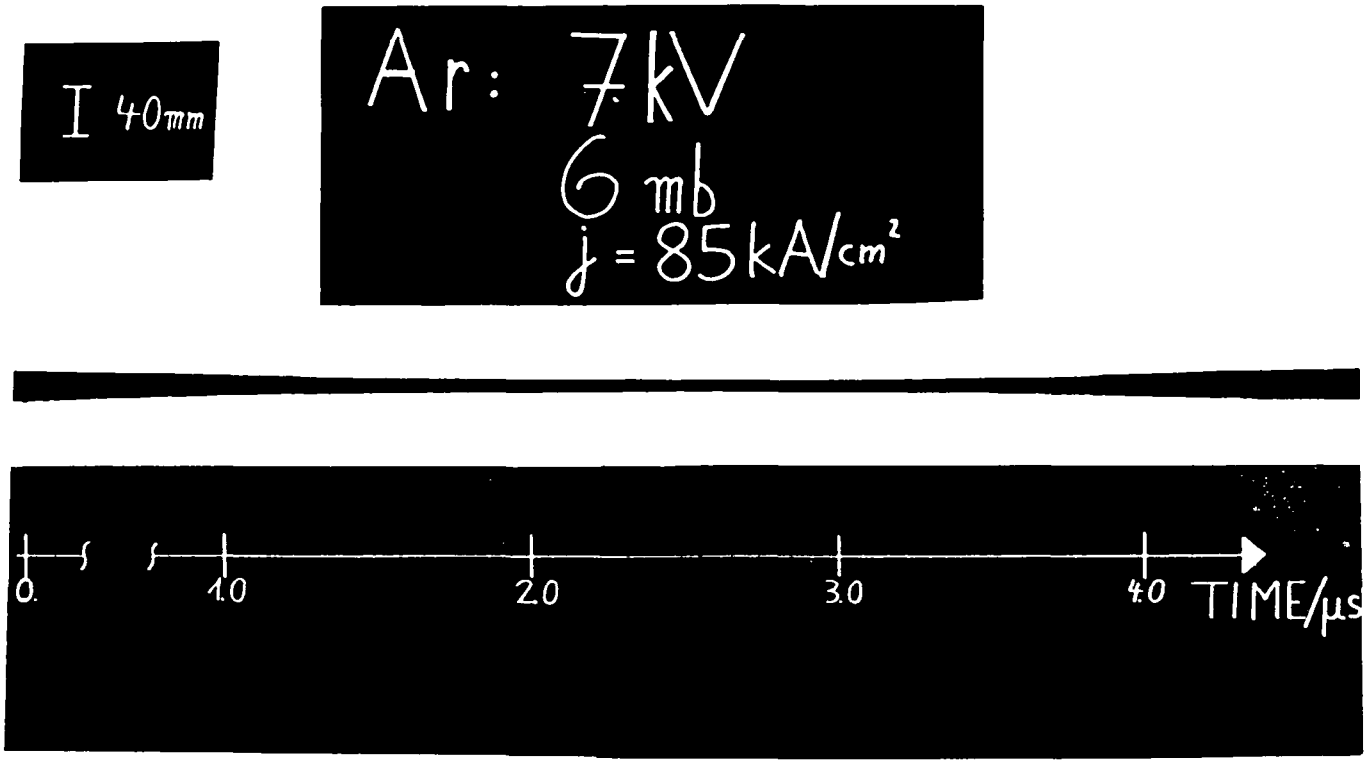

Streakphotograph of first contraction phase (minimum pinch radius ≈ 5 mm).
Stable and uniform discharge conditions exist for more than 1 µs.

Fig. 14

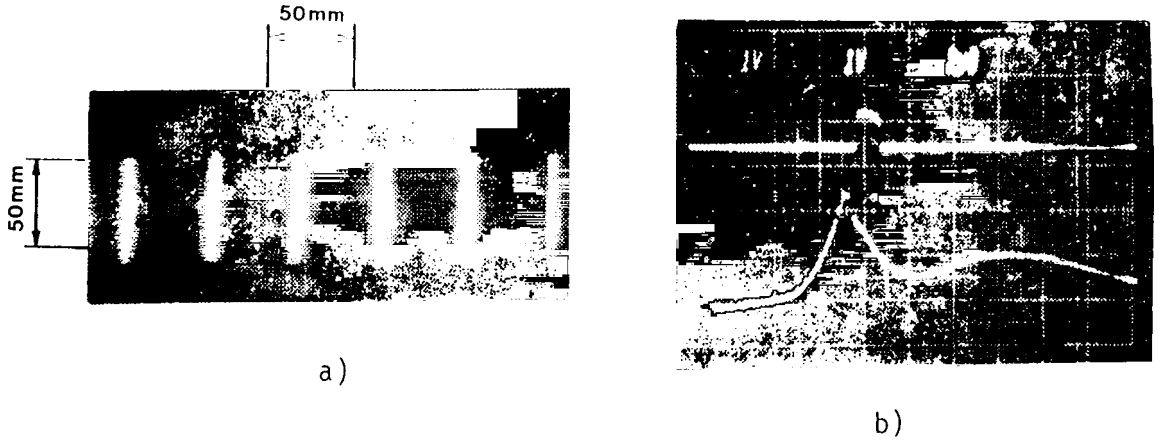

a) Framing photos of pinched plasma column near anode in PL with Ar at 4 mb, U_0 = 7 kV (distance between frames = 12.5 ns).

b) Diff. voltage waveform and trigger pulse for streak camera.

Fig. 15

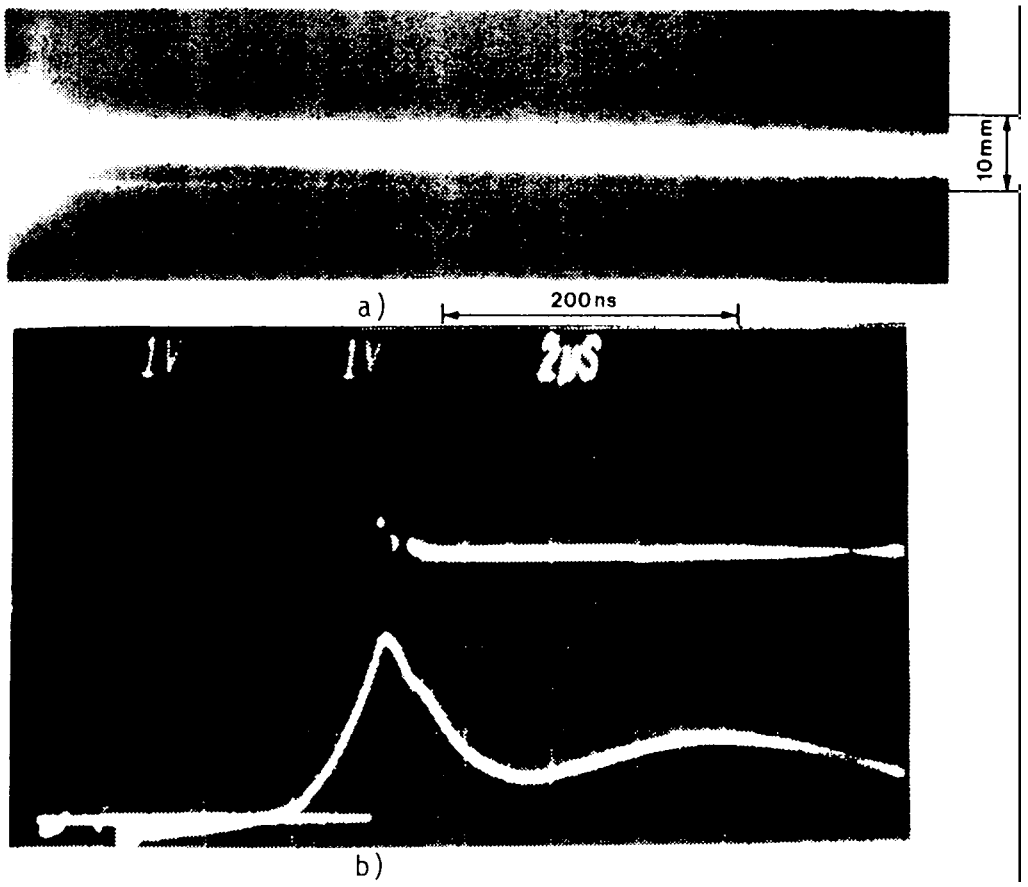

a) Streak photo taken just before maximum contraction.

b) Camera timing pulse in relation to diff. voltage waveform. PL filled with Argon at 4 mb, U_0 = 7 kV.

Fig. 16

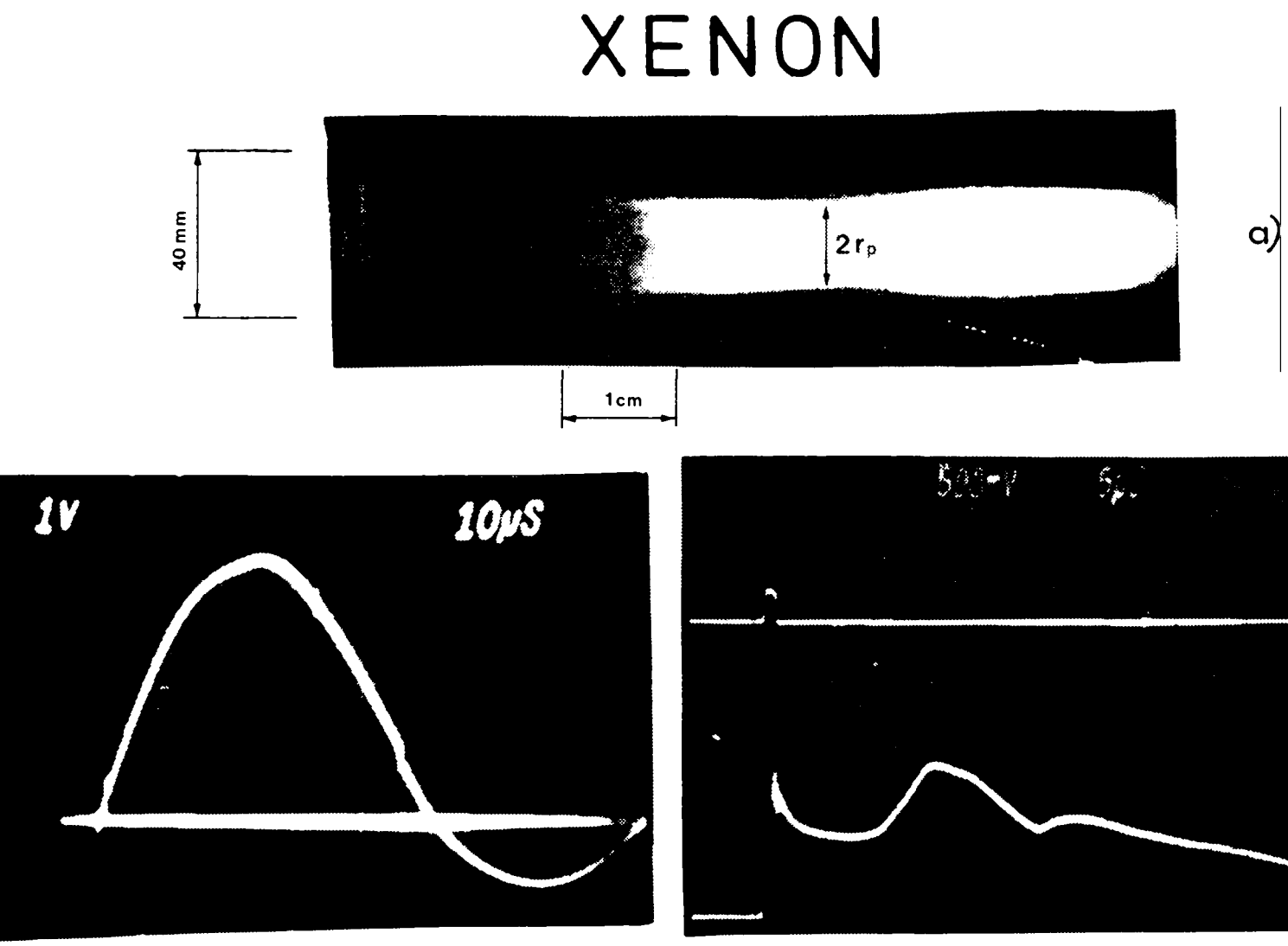

a) Streakphoto of PL with Xe at 10 mb, U_0 = 7kV, streakspeed 3μs/cm
b) and c) corresponding current and diff. voltage waveforms

Fig. 17

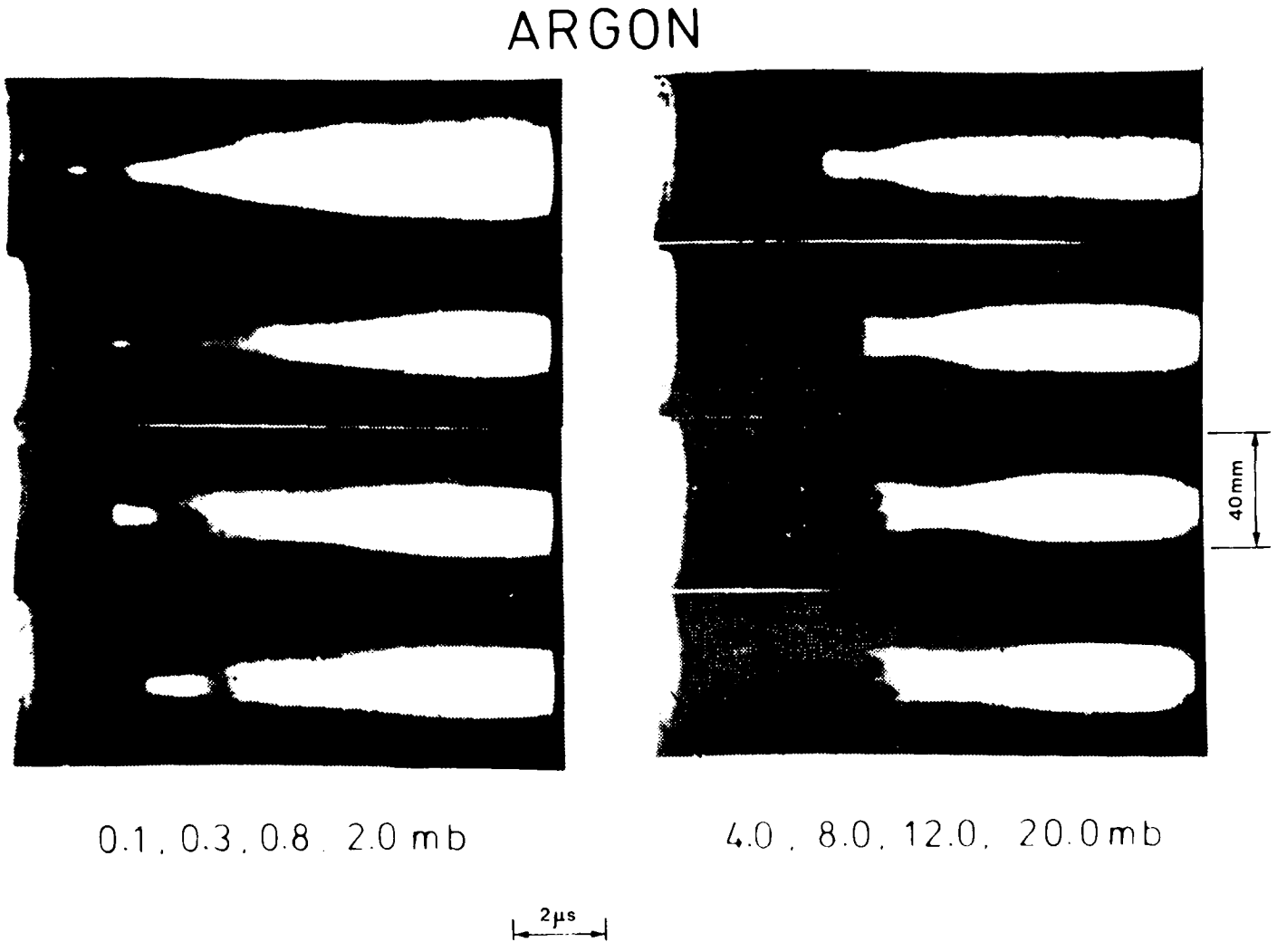

Streak photos of PL filled with Ar at different pressures,
U_0 = 9.0 kV , streakspeed = 2 µs/cm.
Note rising pinch radius and pinch time with rising pressure.

Fig. 18

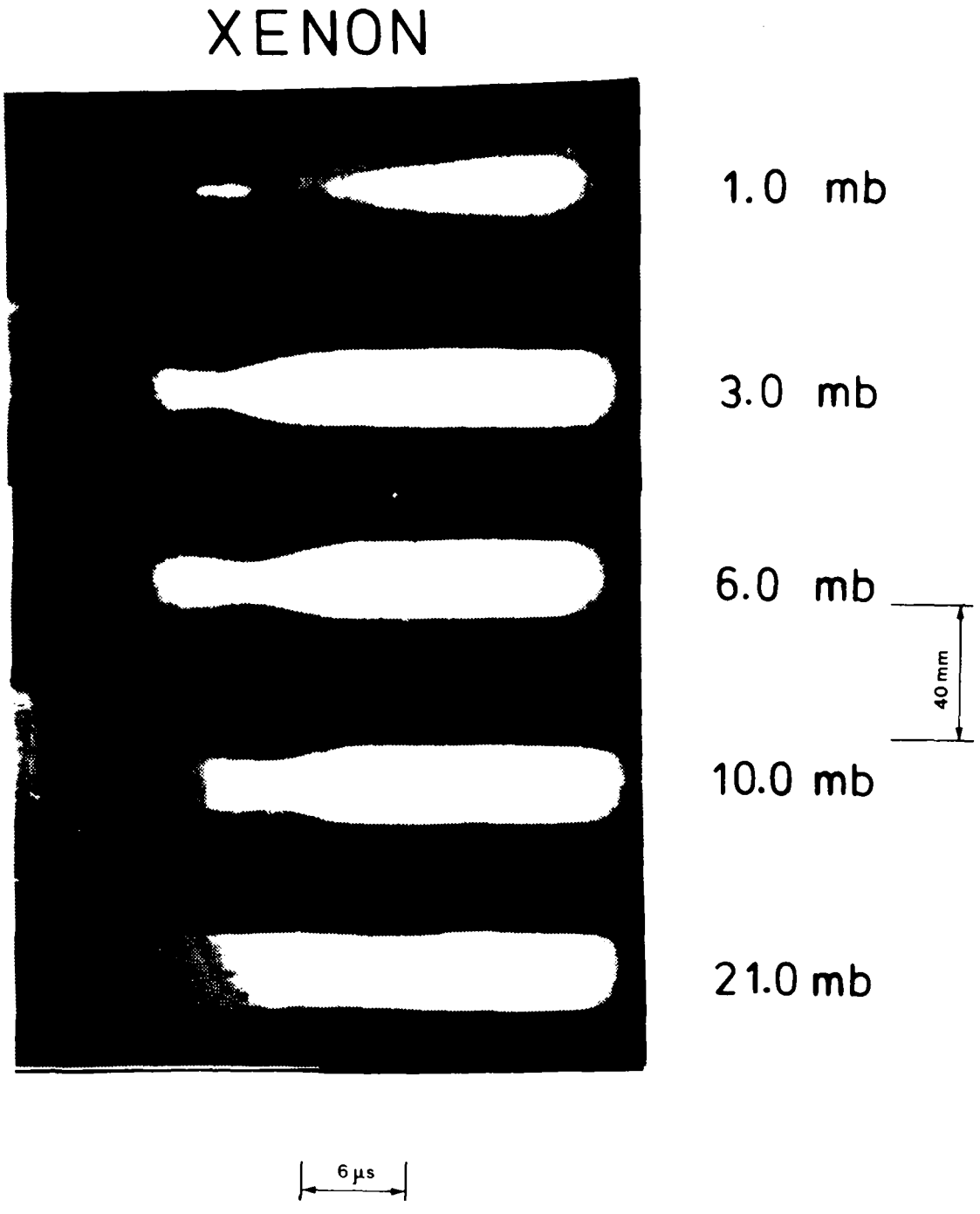

Streak photos of PL filled with xenon at various pressures,
U_0 = 11 kV, streakspeed = 3 µs/cm.

Fig. 19

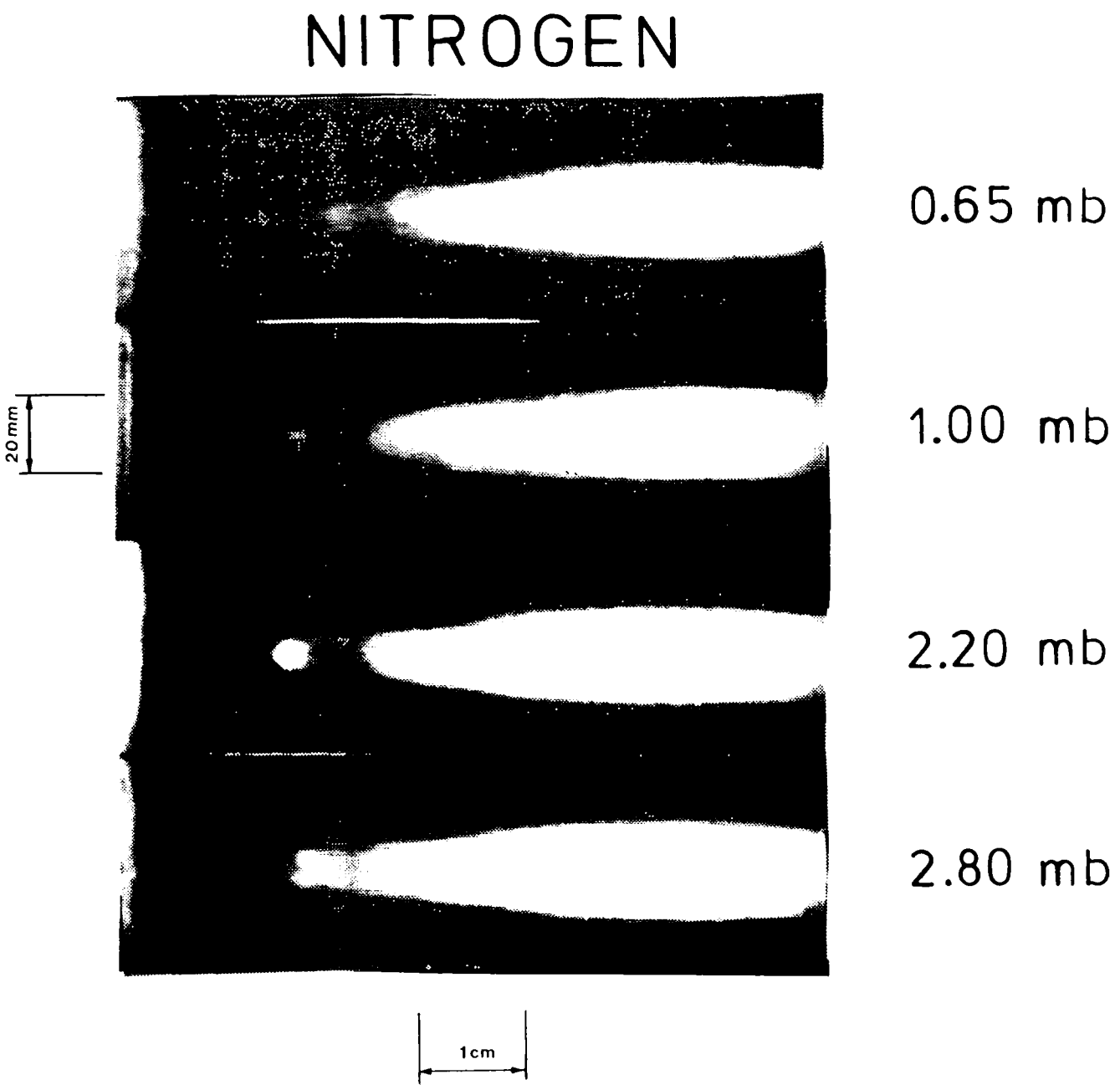

Streakphotos of PL filled with nitrogen at various pressures,
U_0 = 9 KV, streakspeed = 3 μs/cm

Fig. 20

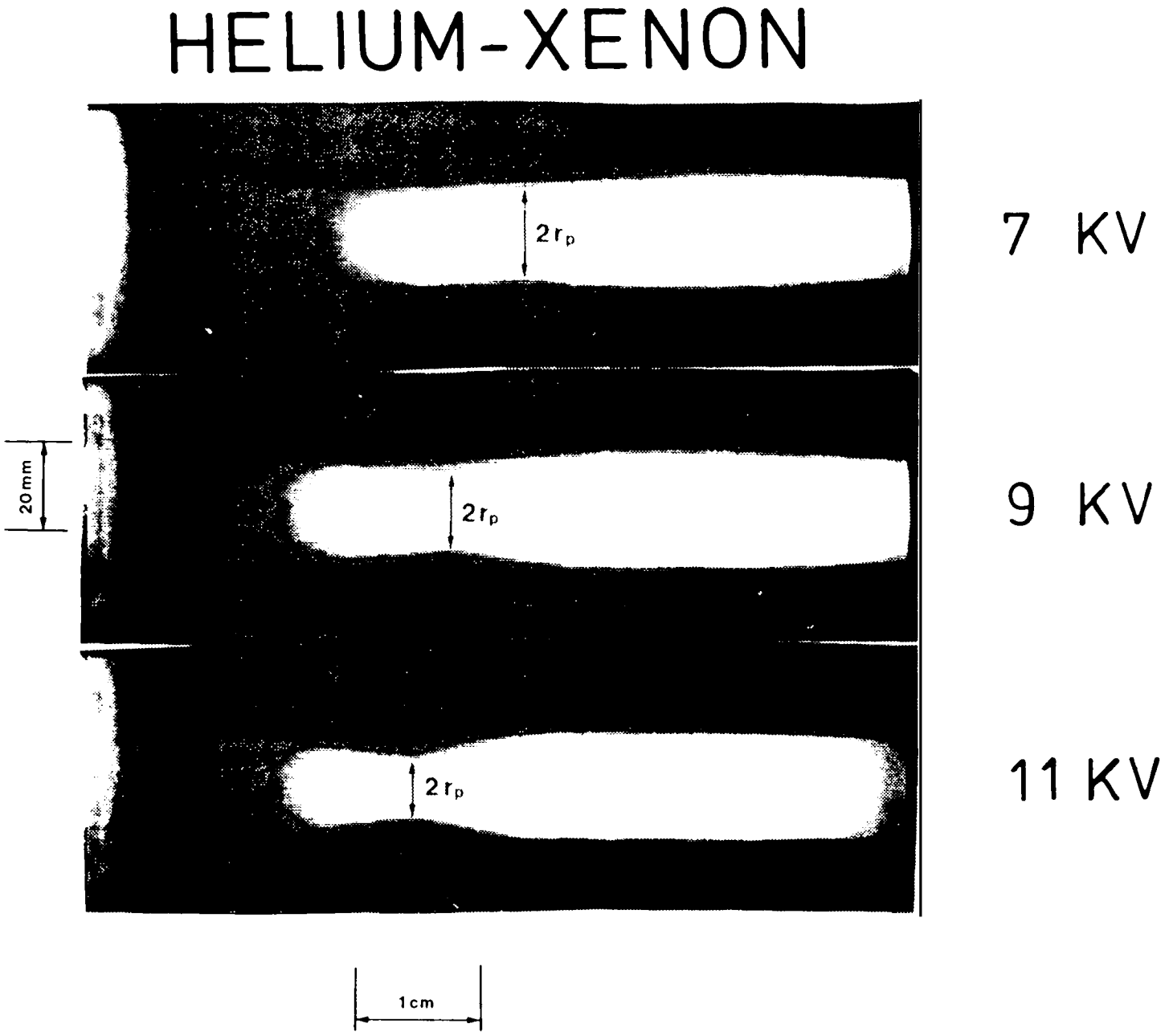

Streakphoto of PL filled with a 50 He/ 50 Xe mixture at 5 mb and pulsed with various charging voltages U_0.
Note decreasing pinch radius and pinch time with rising charging voltage (streakspeed = 3 μs/cm)

Fig. 21

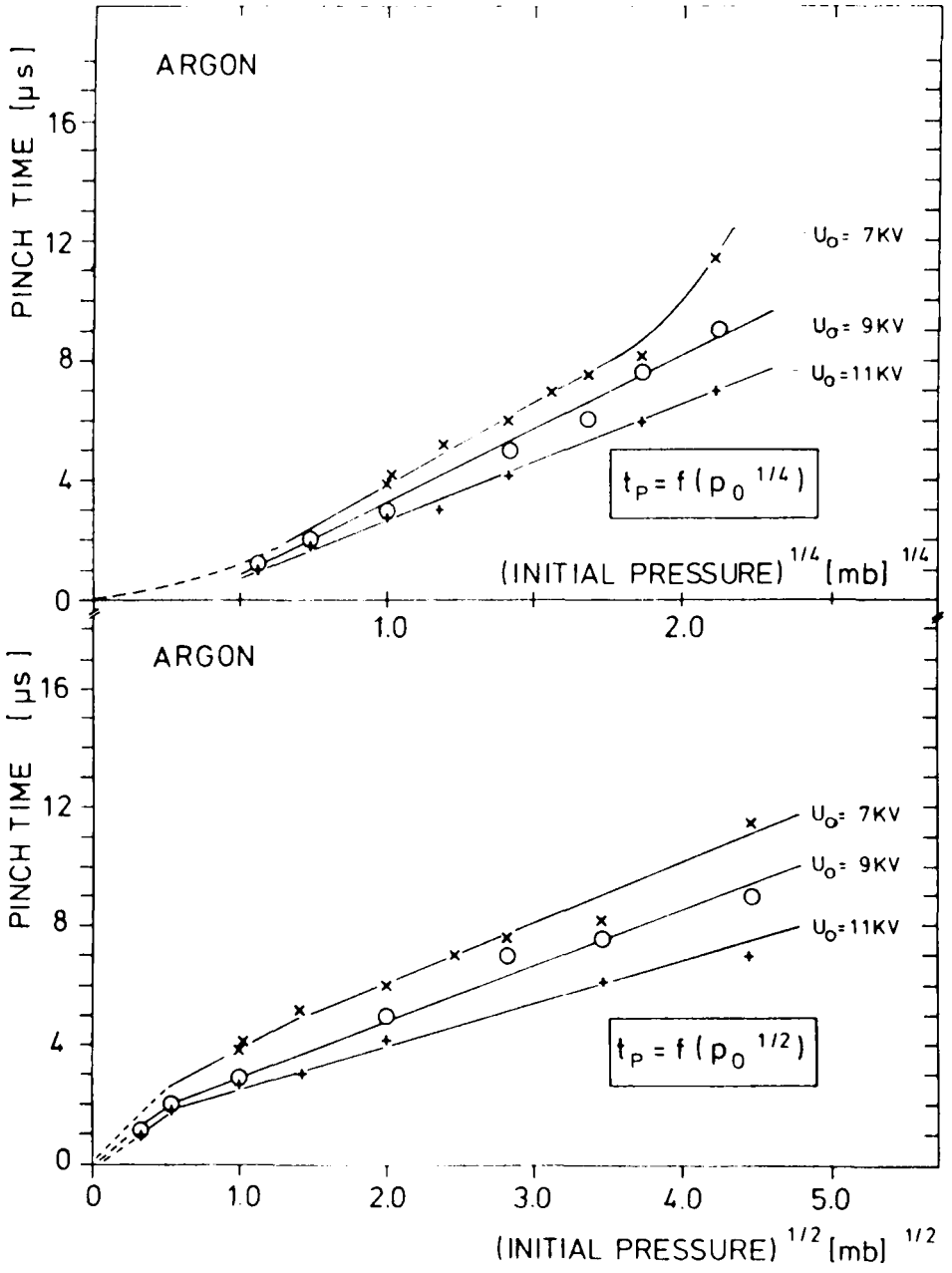

Pinch time from streakphotos and diff. voltage measurements as function of fourth (a) and second (b) root of argon pressure for various charging voltages U_0.

Fig. 22

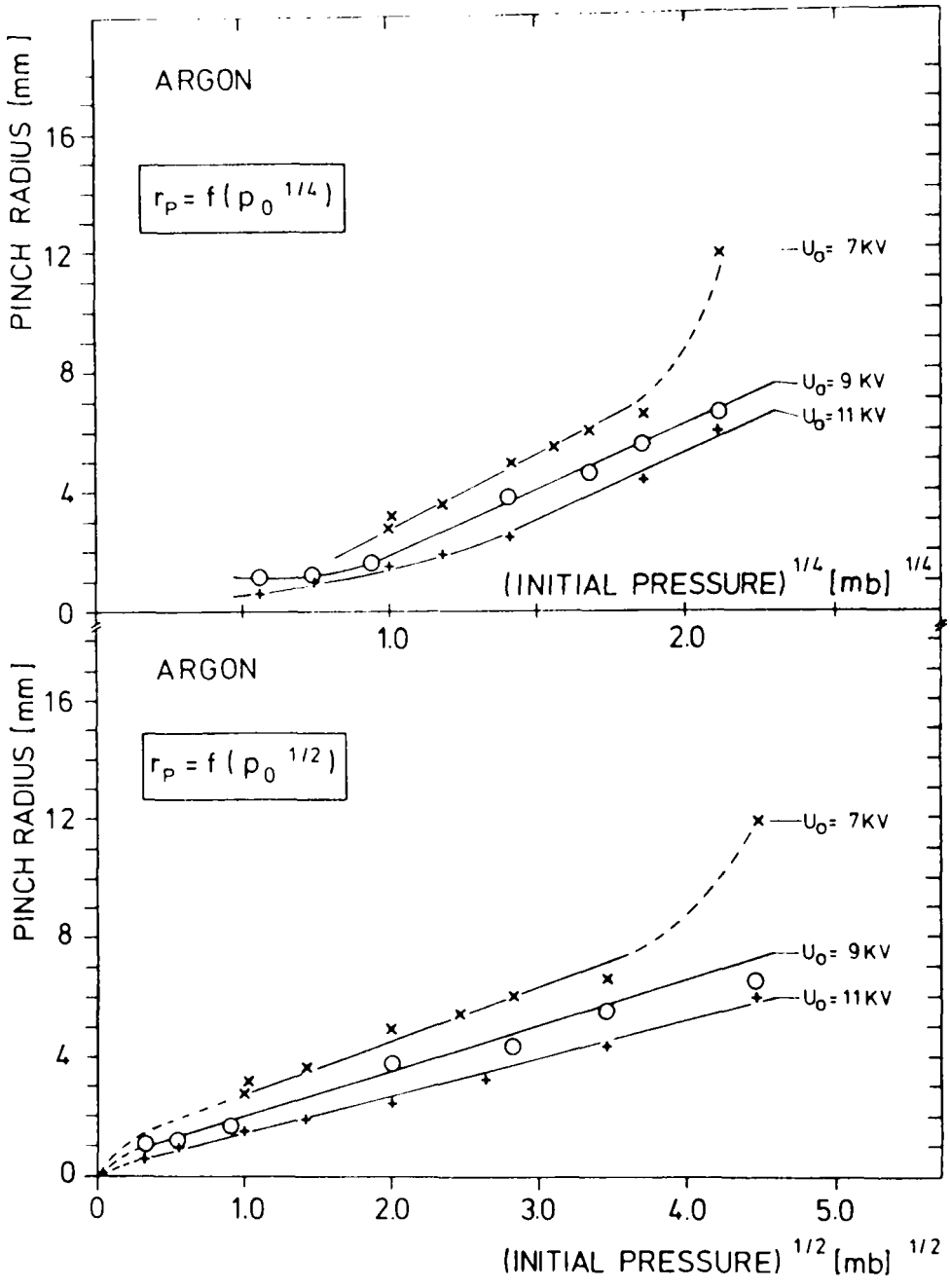

Pinch radius from streakphotos as function of fourth (a) or second (b) root of argon pressure for various charging voltages U_0.

Fig. 23

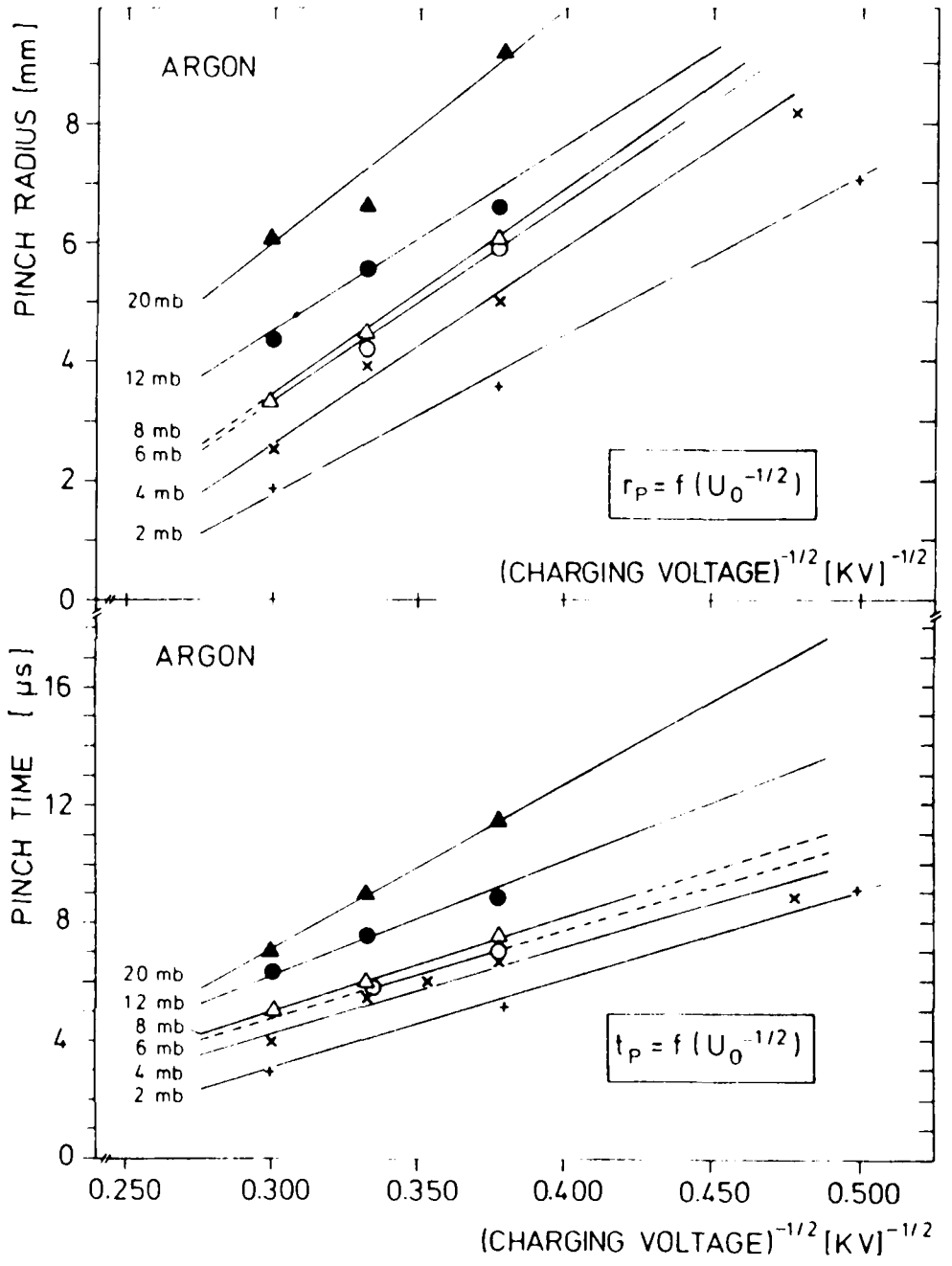

Pinch radius (a) and pinch time (b) as functions of the inverse square root of charging voltage U_0 for various argon pressures.

Fig. 24

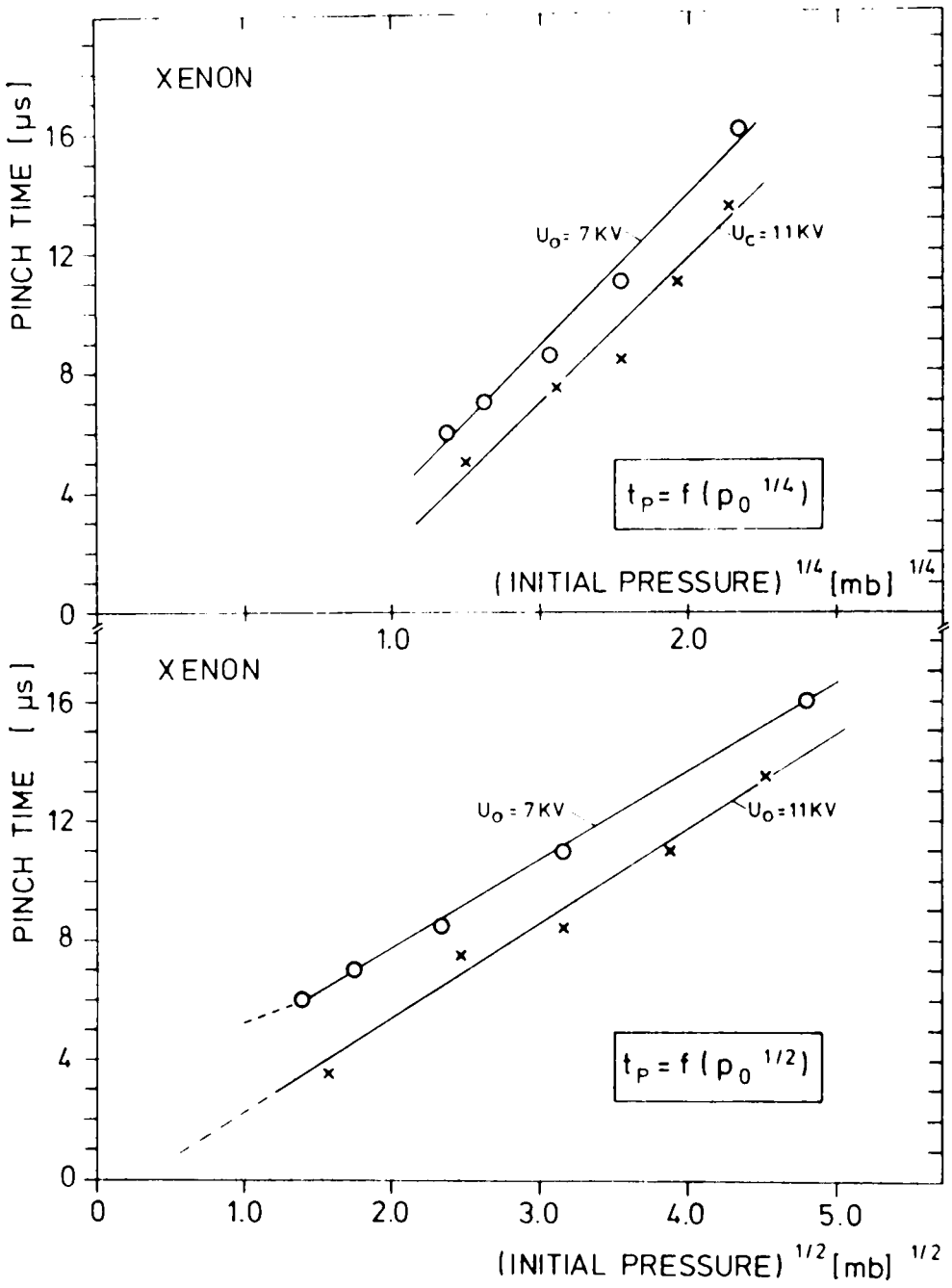

Pinch time from streak and differential voltage measurements as function of the fourth (a) or second (b) root of xenon pressure for 7 and 11 kV charging voltage.

Fig. 25

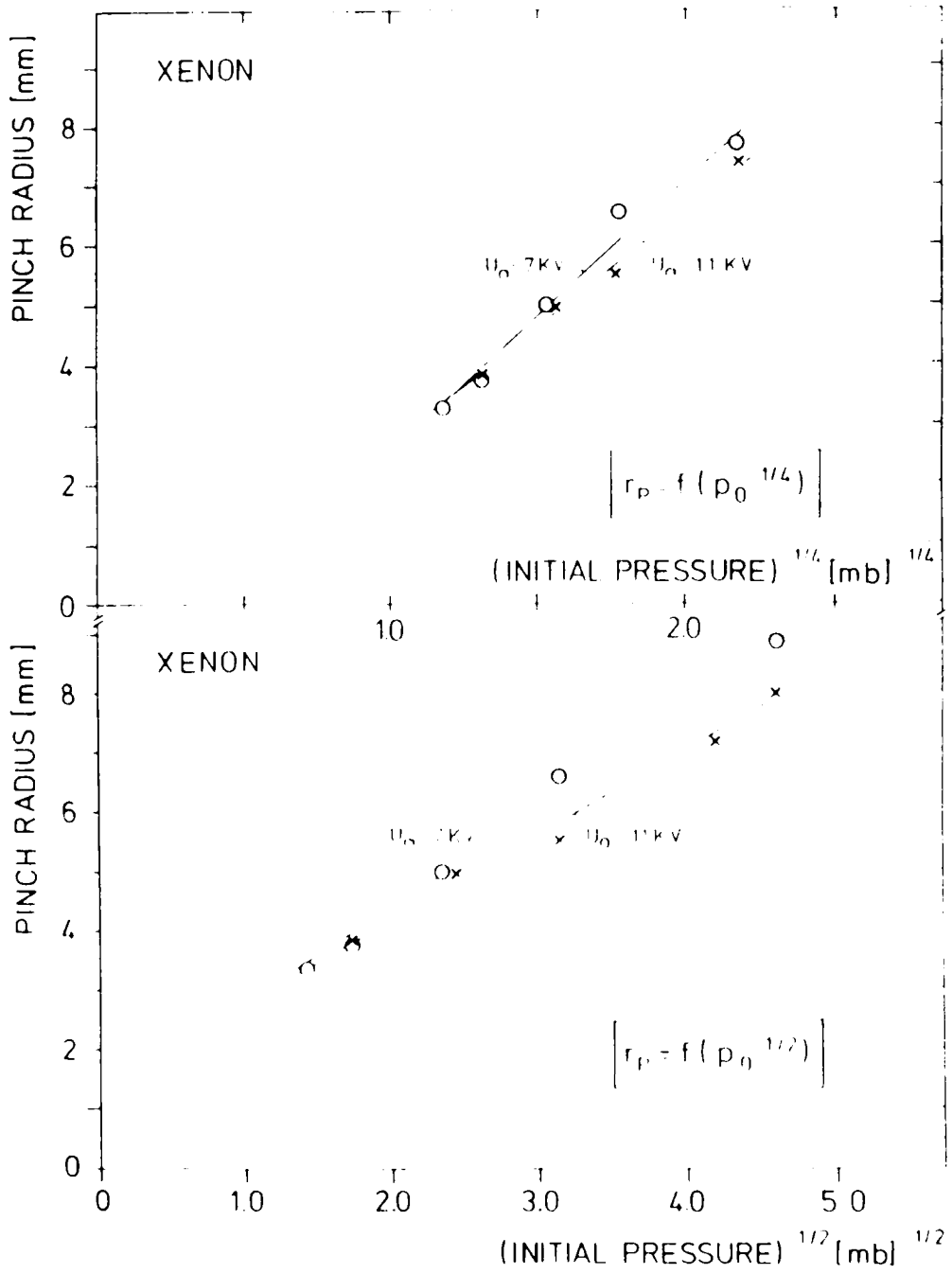

Pinch radius from streak measurements as function of fourth (a) or second (b) root of xenon pressure for 7 and 11 kV charging voltage.

Fig. 26

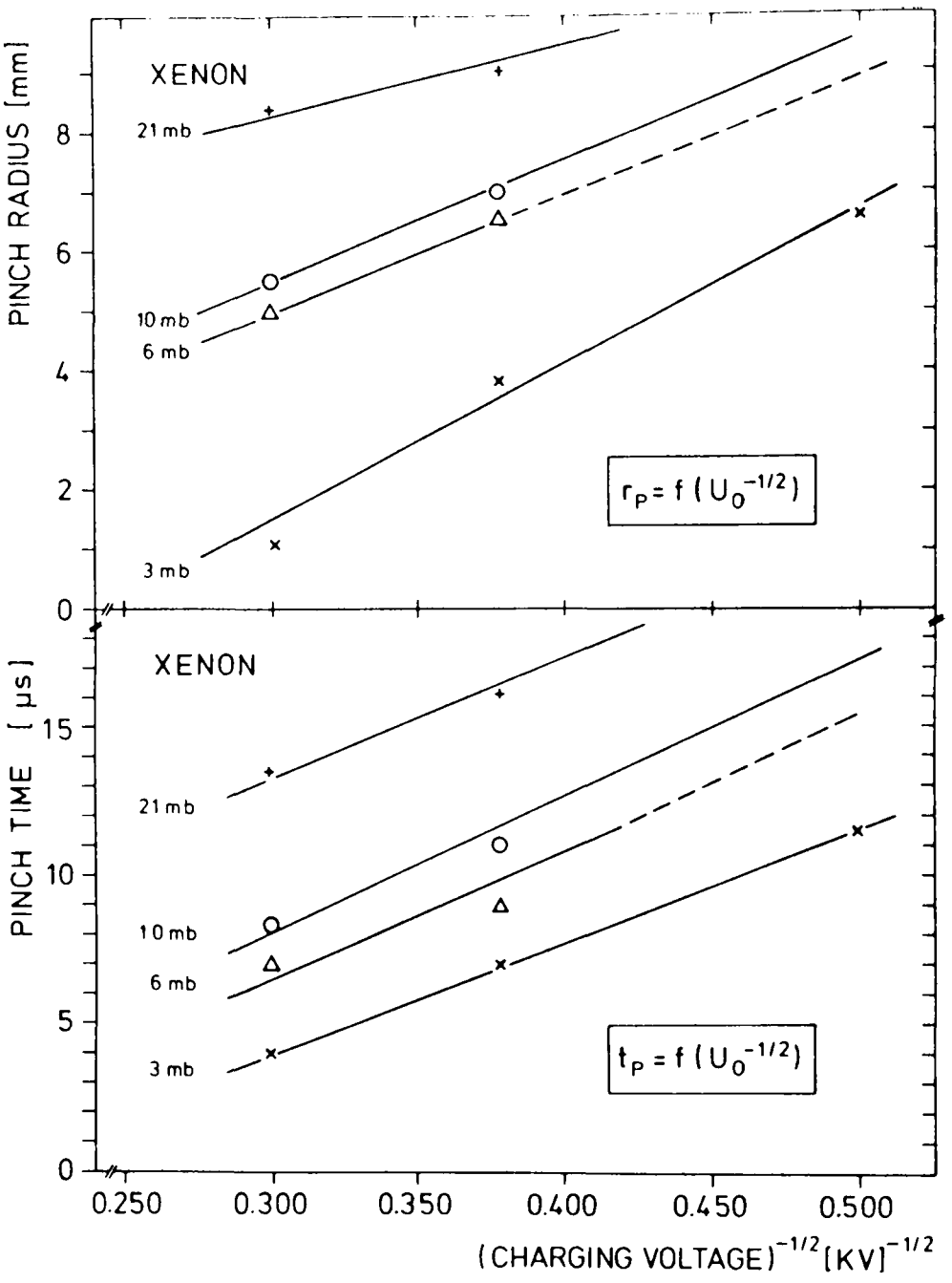

Pinch radius (a) and pinch time (b) as functions of inverse square root of charging voltage U_0 for various xenon pressures.

Fig. 27

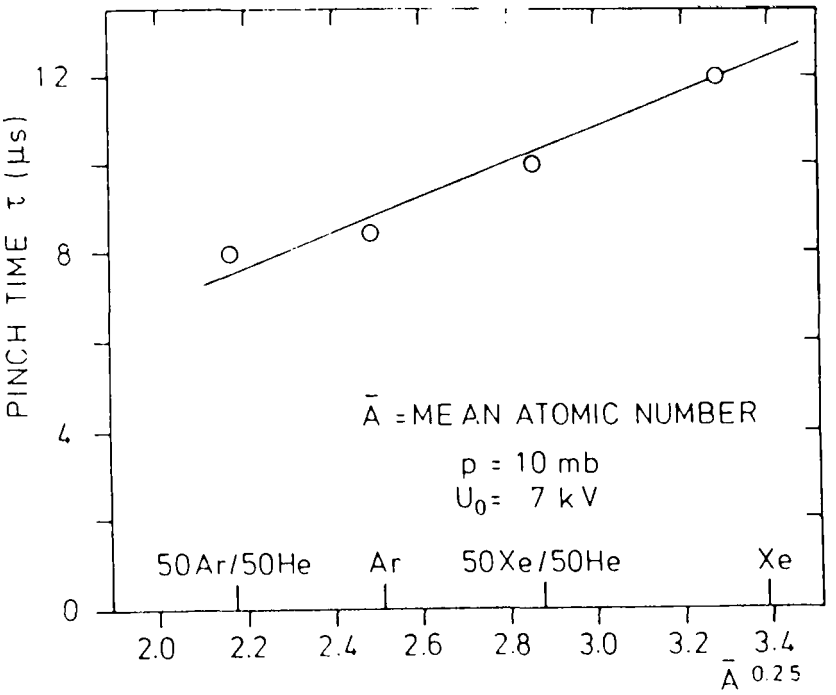

Pinch time as function of the fourth root of mean atomic number.

Fig. 28

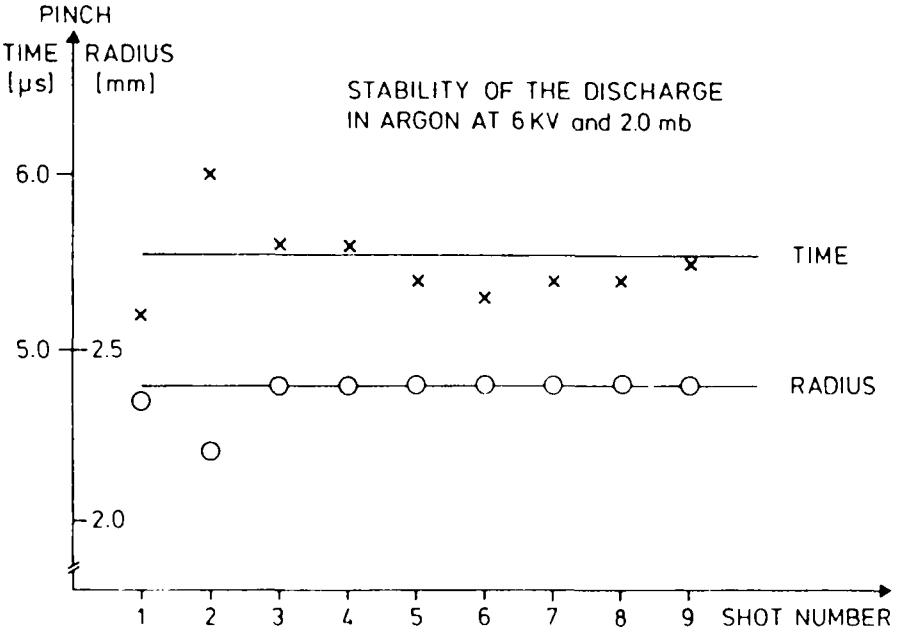

Reproducibility of consecutive discharges after opening PL at atmospheric pressure.

Fig. 29

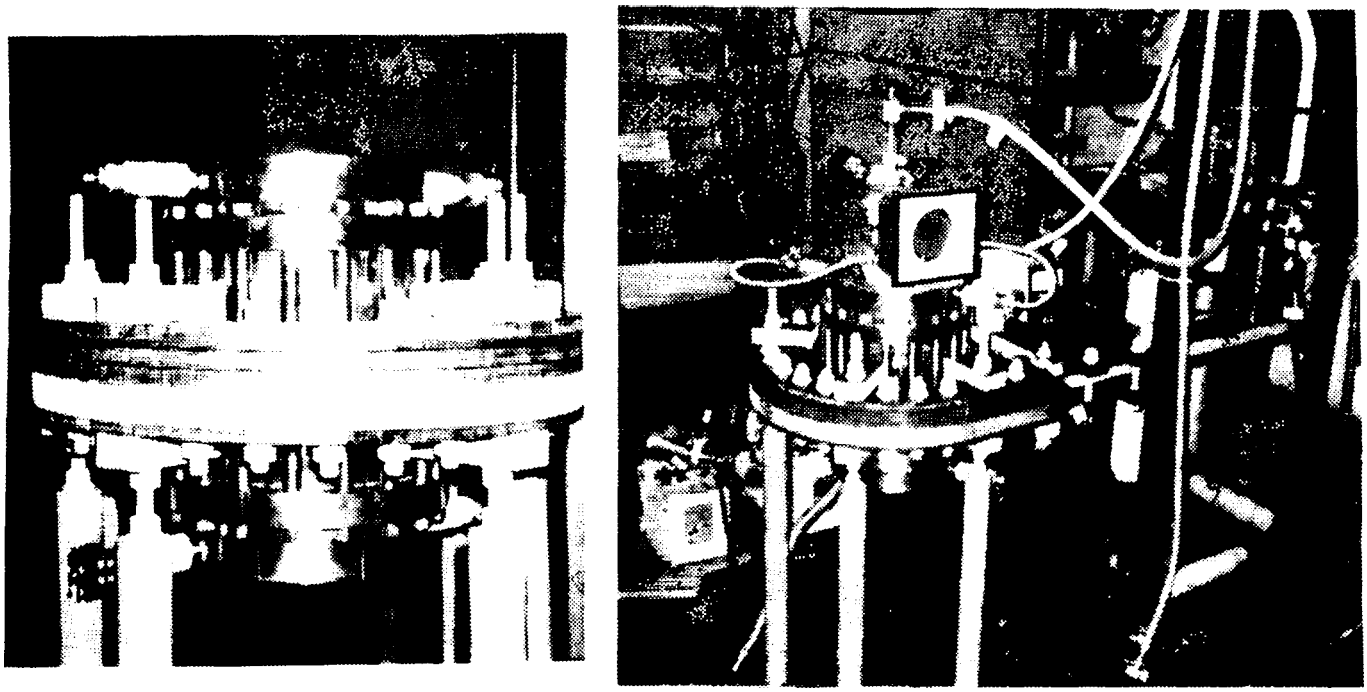

Photo of second plasma lens prototype (inner quartz tube diameter of PL-prototype II = 236 mm).

Fig. 30

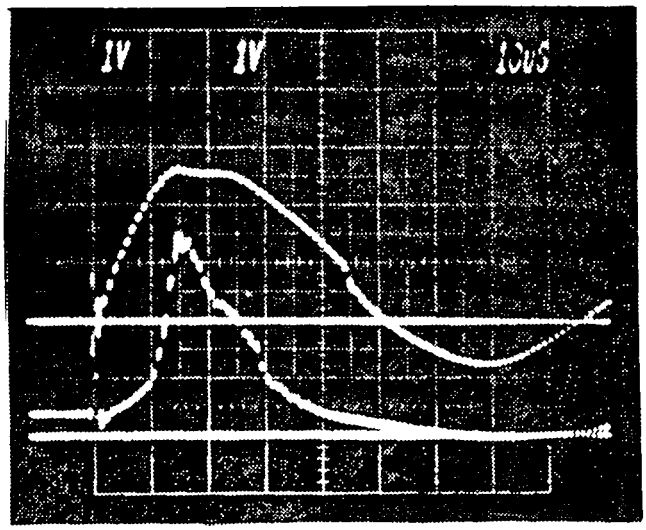

Simultaneous current 42.5 kA/V and diff. voltage (1kV/div) signals of PL prototype II filled with Ar at 0.07 mb, U_o = 8 kV.

Note: Maximum current and pinch phase can be easily made to coincide.

Fig. 31